

# CORTICOTHALAMIC MODELLING OF SLEEP NEUROPHYSIOLOGY WITH APPLICATIONS TO MOBILE EEG

---

Taha Morshedzadeh<sup>1,2,\*</sup>, Kevin Kadak<sup>1,2</sup>, Sorenza P. Bastiaens<sup>1,2</sup>, M. Parsa Oveis<sup>1,7</sup>, Davide Momi<sup>1</sup>, Zheng Wang<sup>1</sup>,  
Shreyas Harita<sup>1,2</sup>, Maurice Abou Jaude<sup>3</sup>, Christopher A. Aimone<sup>3</sup>, Steve Mann<sup>5</sup>, Sean L. Hill<sup>1,4,6</sup>, and John D.  
Griffiths<sup>1,2,4,7,\*</sup>

<sup>1</sup>Krembil Centre for Neuroinformatics, Centre for Addiction and Mental Health, Toronto (*primary affiliation*)

<sup>2</sup>Institute of Medical Science (IMS), University of Toronto

<sup>3</sup>InteraXon Inc., Toronto, ON, Canada

<sup>4</sup>Department of Psychiatry, University of Toronto

<sup>5</sup>Department of Electrical & Computer Engineering, University of Toronto

<sup>6</sup>Department of Physiology, University of Toronto

<sup>7</sup>Institute of Biomedical Engineering, University of Toronto

\*Corresponding author – Email: [taha.morshedzadeh@gmail.com](mailto:taha.morshedzadeh@gmail.com); [john.griffiths@utoronto.ca](mailto:john.griffiths@utoronto.ca);

November 4, 2024

## ABSTRACT

Recent developments in mathematical modelling of EEG enable the tracking of otherwise-inaccessible neurophysiological parameters throughout sleep. Likewise, advancements in wearable electronics have enabled easy & affordable collection of sleep EEG at home. The convergence of these two advances, namely neurophysiological modelling for mobile sleep EEG, can boost preclinical and clinical assessments of sleep. However, this subject area has received limited attention in existing literature. To address this, we used an established model of the corticothalamic system to analyze EEG power spectra from 5 datasets, spanning from research-grade systems to at-home mobile EEG. In the present work, we compare the convergent and divergent features of the data and the estimated physiological model parameters. While data quality and characteristics differ considerably, key patterns consistent with previous theoretical and empirical work are observed. During the transition from lighter to deeper NREM, i) exponent of the aperiodic ( $1/f$ ) spectral component is increased, ii) bottom-up thalamocortical drive is reduced, iii) corticocortical connection strengths are increased. This effect is observed in healthy subjects but is interestingly absent when taking SSRI antidepressants, suggesting possible effects of ascending neuromodulation on corticothalamic oscillations. We further show a month-long increase in REM% in one mobile EEG subject, associated with boosted high-frequency activity in spectra and higher thalamothalamic gains in the model, pointing to possible changes of thalamic inhibition in REM parasomnias. Our results provide a proof-of-principle for the utility and feasibility of this physiological modelling-based approach to analyzing mobile EEG data, providing a mechanistic measure of brain physiology during sleep.

**Keywords** Neural Field Modelling · Electroencephalography · Power Spectral Density · Corticothalamic System · Excitation & Inhibition

## Statement of significance

We employ a physiological model of the corticothalamic circuitry to model the EEG power spectra in sleep. We fit this model to 5 EEG datasets, and demonstrate that while mobile and non-mobile EEG recordings differ in their characteristics and quality, they can both robustly represent the changes along sleep stages using the aperiodic ( $1/f$ ) component. We observe an increased corticocortical connection strength and decreased corticothalamic connection strength as the subject goes into deeper stages of NREM sleep; an effect that is, importantly, not observed in subjects taking SSRIs. This work provides a proof-of-concept for using mathematical modelling, working well for large mobile and non-mobile datasets providing valuable insight into the mechanisms generating sleep EEG.

## 30 1 Introduction

### 31 Sleep neurophysiology and EEG

32 Sleep is a vital and near-universal physiological function, manifested in most of the animal kingdom in a regular  
33 circadian pattern [1, 2]. It is far more than just a state of rest and reduced energy expenditure. States of sleep serve as  
34 a period during which the brain undergoes significant changes, including metabolic homeostasis and recovery [3, 4],  
35 synaptic regulation, and memory consolidation [1, 5]. Disturbances in sleep rhythms can also increase susceptibility to  
36 various types of psychiatric and neurological conditions such as mood disorders, epilepsy, and dementia [6–9]. Despite  
37 these associations, sleep disorders remain highly underdiagnosed clinically, or misdiagnosed as other neurological  
38 ailments [10].

39 The physiological state of the brain moves through a complex trajectory of dynamical regimes during a night's sleep.  
40 These changes evolve on the timescale of tens of minutes, and their electrical footprints are reflected in (and are indeed  
41 defined by) electroencephalography (EEG) recordings. Polysomnography (PSG), is one of the most widely-used  
42 methods for evaluating sleep in the clinical setting. It involves the concurrent monitoring of EEG, electromyography  
43 (EMG), electrooculography (EOG), movement, and respiration. Sleep stages are defined in terms of the properties  
44 of EEG time series data over standard (30s) windows, and the time series of the stages for the successive windows  
45 forms the hypnogram. This data is typically evaluated over a single channel, following the –mostly correct– assumption  
46 that brain activity changes similarly across all EEG channels during sleep [11]. Each of these stages has characteristic  
47 phenomenological definitions defined by the common sleep staging standards [12, 13]. Although it has strong diagnostic  
48 and prognostic utility [14, 7, 15–17], classical sleep staging is highly constrained as it is limited to only 5 values (the 5  
49 stages W, N1, N2, N3, REM) to capture the vast continuum of brain states in sleep. This problem is further exacerbated  
50 by the highly subjective interpretation of different stages by human scorers, which has led to considerable inter-expert  
51 variability [18, 19]. Therefore, it is crucial to augment this information with more detailed quantitative approaches for  
52 evaluating brain activity trajectories in sleep.

53 Power spectral estimation is one of the fundamental methods for studying the characteristics of a time series signal  
54 across different frequencies. Studying the EEG power spectral density (PSD) in the same 30-second windows used for  
55 sleep staging can provide us with a more high-dimensional evaluation of brain states over these intervals. EEG PSDs can  
56 be reliably described in terms of two main components: i) A background  $1/f^n$  trend, understood to be non-oscillatory  
57 or 'aperiodic', and defined by its exponent and offset, and ii) An oscillatory component which is highly periodic,  
58 featuring well-defined attributes such as frequency, amplitude, and bandwidth. The aperiodic component is an intrinsic  
59 feature of many natural processes, and is believed in the neuroscientific context to reflect variable excitatory/inhibitory  
60 balance [20]. It has also been linked to cognitive decline in ageing [21], cognitive speed [22], and movement [23].  
61 Periodic activity is traditionally examined in the frequency bands delta (0.5-4 Hz), theta (4-7.5 Hz), alpha (7.5-12  
62 Hz), beta (16-30 Hz), and gamma (>30 Hz). During wakefulness, the brain exhibits high-frequency low-amplitude  
63 activity, and as the subject transitions to NREM sleep, the activity transitions into a low-frequency high-amplitude

64 pattern.[24, 25]. The transition from lighter to deeper NREM sleep is associated with increased slope of the EEG  
65 power spectrum, along with increases in the amplitude of the delta band and a decrease in the amplitude the alpha band  
66 [26]. Wakefulness also is signified by a presence of alpha and gamma peaks, and REM (rapid eye movement) sleep is  
67 correlated with increases in gamma and theta but not alpha peaks [27].

68 The principal brain structure that drives brain state changes during sleep, including our measurement of them with  
69 EEG, is the corticothalamic system [28–30]. Different stages of sleep have been linked to changes in corticothalamic  
70 activity [29, 31–34] and to changes in the periodic and aperiodic components of the EEG signals over those changes  
71 [35, 36, 34, 37]. For instance, the transition from wakefulness to N1 sleep is also characterized by an increase in the  
72 slope of the  $1/f$  component and the low-frequency band powers [35, 36], which is itself observed to be associated with  
73 corticothalamic communication [30].

74 Sleep stage N3, also known as slow-wave sleep (SWS), is understood as the deepest stage of NREM sleep, showing  
75 strongly synchronized cortical activity in the infra-slow (<1 Hz) and delta (1-4 Hz) frequency bands. This synchronized  
76 cortical activity has been shown to be driven locally through corticocortical connections, and with reduced thalamocorti-  
77 cal input [31, 38–40]. Interestingly, 1 Hz transcranial magnetic stimulation (TMS) in the cortex can effectively entrain  
78 this 1 Hz cortical oscillation around the stimulation site [41], indicating that cortical activation is the primary source  
79 driving this oscillation. Synaptic homeostasis and long-term potentiation (LTP) have also been found to occur strongly  
80 in SWS [5, 33], and brain stimulation at this stage can trigger memory replays and improve memory recall [42].

## 81 Mathematical modelling of sleep-wake dynamics

82 This deep foundation of experimental knowledge in neuroscience across multiple species, spatial scales, and observable  
83 phenomena, provides a strong motivation for the development and use of mathematical models that explain sleep EEG in  
84 terms of their underlying neurophysiological processes across the units of the corticothalamic circuitry. One of the most  
85 widely used and extensively studied models of this kind to date was introduced by Robinson et al. [30], which describes,  
86 at the mesoscopic spatial scale, a four-node corticothalamic network containing the thalamic relay, thalamic reticular,  
87 cortical excitatory, and cortical inhibitory neural populations. With this structure, the Robinson model has proved highly  
88 capable of replicating measured EEG time series and power spectra [30, 43–45], with applications including evoked  
89 potentials [46, 47], alpha rhythms [48], and sleep & arousal [49, 50], to name only a few. In a 2015 paper, Abeysuriya  
90 et al. demonstrate the use of this model to study the trajectories of physiological brain states expressed through the  
91 EEG, across a night of sleep [51]. By fitting the model-generated power spectra to those observed in empirical EEG,  
92 circuit mechanisms such as corticocortical, corticothalamic, and intrathalamic connection strengths can be estimated  
93 from 30-second windows rolling throughout the night, and their changes compared against separately-scored PSG  
94 classifications. In this way, mathematical modelling of corticothalamic system dynamics can be used to enrich the  
95 observations made via classical sleep stages and conventional power spectral analysis.

96 **Emerging mobile neurotechnologies for sleep EEG measurements**

97 One of the most significant technical developments in the field of EEG over the past decade has been a suite of hardware,  
98 software, and commercial innovations leading to the widespread availability of low-cost ("consumer-grade") wireless  
99 mobile EEG devices. The lower price tag, smaller footprint, use of flexible components such as conductive rubber and  
100 conductive fabric, and more streamlined setup of these systems hold great promise for scientists and clinicians needing  
101 to access larger samples of subjects and over many more nights than is possible with traditional in-lab sleep EEG  
102 assessments. Two of the most established mobile sleep EEG headsets on the market today are Muse S by Interaxon  
103 [52] and Dreem by Beacon Biosignals [53]. Although, these products face stiff competition from other startups that  
104 with smaller but increasing market share, such as Cerebra [54], URGONight [55], IDUN [56], and Elemind [57], along  
105 with major consumer electronics companies such as LG Electronics (sleepwave.ai) that are looking to enter the mobile  
106 sleep EEG market.

107 This approach can enable an easier and more affordable overnight recording of sleep EEG at home or in the research  
108 lab. The easier setup and reduced cost can readily enable the researchers to make recordings over more repeated nights  
109 and for a larger population.

110 **Characterizing trajectories of activity in healthy vs. unhealthy sleep**

111 The mathematical models of EEG activity enable us to reconstruct an embedding space underlying the changes in EEG  
112 activity observed in sleep. Fitting these models to repeated recordings from a larger sample size of participants  
113 enable us to catalogue a rich set of ranges and the trajectories of the physiological parameters from the model in various  
114 nights of sleep. Not only can applying such mathematical models to repeated recordings from a larger sample size of  
115 participants help us characterize the ranges of normative parameters correlated with good restorative sleep, but the  
116 repeated recordings can also help us detect the ranges associated with sporadic changes in sleep quality or potential  
117 parasomnias that require continuous monitoring [58, 59].

118 Certain sleep EEG patterns are correlated with mood, anxiety, and other mental health factors, but this area remains  
119 understudied due to the logistical challenges of the repeated recording of sleep EEG over extended periods, especially  
120 from subclinical, at-risk, or asymptomatic populations who are at home rather than in controlled, hospitalized settings  
121 [60–62]. Mobile EEG systems are key in bridging this gap, since they make continuous and long-term monitoring of  
122 sleep EEG outside of the clinical environment feasible.

123 Additionally, there is significant night-by-night variability in sleep within the same individual. Collecting extensive  
124 nightly data from the same person allows the identification of consistent, robust patterns unique to that individual, and  
125 it reduces the effects of these stochastic fluctuations. Dreaming is an example of a sparse sleep event which varies  
126 night-by-night, is associated with many determinants of mental and physical health [63, 64], and its actuation is strongly  
127 affected by the level of comfort in sleep. These factors make it a prime example of a topic that is best investigated using  
128 large-sample-size longitudinal mEEG recordings, as evidenced by ongoing data collection projects such as [65]

129 Brain states undergo semi-regular trajectories and cycles of changes through a night of sleep—which we describe at a  
130 phenotypical level as the hypnogram of the sleep stages. These variations are reflected by the changes in aperiodic and  
131 periodic components of the EEG activity in the power spectral domain. Therefore, we can attain a trajectory of the  
132 parameters underlying those brain states suggested by the corticothalamic model. Beyond mapping these parameter  
133 trajectories to various health or disease states, various interventions and treatments can alter the ranges and trajectories  
134 of these parameters in a unique way, which could be captured via the parameter trajectories describing underlying  
135 physiological state transitions of the brain.

136 In summary, by fitting many such sleep recordings to the mathematical model, we can characterize the embeddings  
137 and their transitions associated with *healthy* sleep, and detect canonical patterns of activity associated with this state.  
138 Moreover, we can examine parameters derived from fitting the model to *unhealthy* sleep EEG to understand how these  
139 key patterns deviate and where disruptions occur. And lastly, we can observe again how various types of *interventions*  
140 can change brain activity.

#### 141 **Personalized medicine informed by physiological modelling of mEEG data**

142 In the recent years, there has been a welcome shift in the computational neuroscience towards implementing the  
143 mathematical models of brain activity to *simulate* an individual's brain activity in health and sleep. This has especially  
144 been explored in brain stimulation research where customized simulations of each person's brain, informed by its  
145 connectomics, are used to predict the effects of the stimulation that is to be delivered. Lang et al. [66] provide a  
146 thorough review of such approaches in Neurosurgery. For instance, a "Virtual Epilepsy Patient" can be simulated to  
147 help detect the epileptogenic zone and devise various surgical and therapeutic interventions [67, 68].

148 The benefits of such modelling approaches is not just limited to the clinical implementation by the bedside. Rather, it  
149 can even be used to assist with the development of new therapeutic choices. An example of such work is demonstrated  
150 by Haas et al. [69], where *in-silico* simulated experiments using biophysical models of the human cortex correctly  
151 predicted the inefficacy of a certain new drug in trial even better than the animal models the drugs where tested on.

152 Utilizing the data from each individual, we can build a *personalized* simulation of their brain in sleep, which has a  
153 customized range and set of properties associated with their sleep. This can not only assist with the diagnostic process,  
154 but can also enlighten us on the underlying processes giving rise to these drops in sleep quality, and also help design  
155 new treatments and monitor & predict the prognostics of the treatment response.

#### 156 **Present work**

157 The recent advances cited above in our fundamental understanding of sleep neurophysiology, our ability to formulate  
158 and model it mathematically, and in the emergence of new technologies promising to radically up-scale the accessibility  
159 of EEG-based sleep monitoring, prompt a series of important research questions at the intersection of these topics.  
160 Previous work on personalized medicine through mesoscopic modelling of the brain has been limited to data that is

161 collected in lab and in clinical departments—and we aimed to study whether we can utilize mobile EEG in the same way  
162 to develop personalized models of brain activity in health & disease.

163 This was the focus of the present study. Selecting several widely used open-access research- and consumer-grade  
164 sleep EEG datasets, we used power spectral analysis to first evaluate the changes to periodic and aperiodic spectrum  
165 components across sleep stages during the night of sleep, assessing the performance of different EEG systems in  
166 capturing variations in physiological brain states. We then fit the Robinson corticothalamic model to these EEG power  
167 spectra, with a view to studying mechanisms underlying these physiological states over sleep stages, and evaluating their  
168 correlations to the depth of NREM sleep. Lastly, we used health data from one of the analyzed cohorts to investigate  
169 the correlations of model-estimated neurophysiological parameters with specific mental & physical health biomarkers.

170 **2 Methods**

171 **2.1 EEG Datasets**

172 We used EEG data from multiple sources, described in the following. All datasets were acquired according to the ethics  
173 board regulation at the hosting institutions. They were accessed and used in accordance with their relevant licences and  
174 data-sharing agreements. The left frontal, central, or temporo-parietal channels were used in each dataset, specifically  
175 F3 or adjacent 10/20 system locations, subject to availability and data quality.

176 **2.1.1 Sleep European Data Format - Extended (Sleep-EDFX)**

177 We used 197 recordings from 185 subjects (97 female / 78 male, mean age 54.7), which were recorded in the time span  
178 of 1987-1991 and 1994 using portable Walkman-style cassettes at home [70, 71]. The accessed data had been digitized  
179 from the analog signal at the sampling rate of 100 Hz. In this dataset, 153 of the subjects had no previous health  
180 conditions and 44 were generally healthy but had trouble sleeping. We accessed the dataset through PhysioNet [72],  
181 acquiring the version last updated in 2018. We selected the data from the Fpz-Cz electrode channel for this work. The  
182 sleep stages were originally marked according to the Rechtschaffen & Kales (R&K) method [13], and were transformed  
183 into the AASM standard for further use in this project. In this paper, we will refer to this dataset as EDF-X for brevity.

184 **2.1.2 Dreem Open Datasets (DOD)**

185 This dataset includes 80 PSGs collected using a research-grade PSG setup from 80 subjects (54 male / 26 female, mean  
186 age 42.39). The dataset was curated by Dreem, a manufacturer of sleep EEG headsets, to benchmark automatic sleep  
187 staging methods [73, 74]. The data was sampled at 250 Hz and scored by sleep professionals based on the 2007 AASM  
188 manual. This dataset is comprised of two sections: 25 healthy subjects recorded in Bretigny-Sur-Orge, France, over 12  
189 mastoid-referenced EEG channels; and 55 at Redwood City, CA, USA, from subjects with Obstructive Sleep Apnea  
190 (OSA), with 8 mastoid-referenced EEG channels. We used the Fp2-O2 channel data from this dataset for the current  
191 project.

---

192 **2.1.3 Nap-EEG Dataset**

193 This dataset was acquired from a healthy cohort of 22 individuals (16 male / 6 female; mean age  $25.5 \pm 7.03$ ). The  
194 data was recorded between 10:00 and 17:00 over 1 to 2 consecutive days at the City College of New York, totalling  
195 41 recordings. Subjects took a high- or low-load cognitive task and then took a nap for 30 minutes, where their EEG  
196 would be recorded over 64 channels of EEG and 2 channels of EOG, sampled at 1.5 KHz [75]. The data includes sleep  
197 stages and 2528 sleep spindles manually annotated, according to the AASM system. The dataset was accessed through  
198 the Open Science Framework (OSF) [76]. The PO8 channel data was chosen for the purpose of this project.

199 **2.1.4 Wisconsin Sleep Cohort (WSC) Dataset**

200 The WSC dataset is recorded from a large cohort of state employees in Wisconsin, United States. We requested and  
201 accessed the standardized dataset through the National Sleep Research Resource (NSRR) [77, 78]. This set includes  
202 2570 recordings from 1123 subjects. This is a longitudinal data set in which the same subjects came to the sleep lab  
203 every 4 to 5 years for a PSG recording. Each subject has 1 to 5 EEG recordings through the years, each approximately  
204 4.5 years apart on average (mean  $4.54 \pm 1.50$  years) between 2000 and 2015. The percentage of subjects with 1, 2, 3, 4,  
205 and 5 recordings was respectively 32.5%, 17.1%, 39.6%, 10.6%, and 0.2%. The subjects were 37 to 85 years old (mean  
206 age  $59.82 \pm 8.49$ , 1385 male / 1185 female). The 6 recording EEG electrodes were referenced to the ipsilateral mastoid  
207 electrodes and sampled at 100 Hz for the data from 2000 - 2009, and at 200 Hz from 2009 to 2015. This dataset also  
208 includes a large variety of mental and physical health information, such as the Zung Depression Scale, anxiety scales,  
209 caffeine consumption, number of recent nights with insomnia, blood pressure disorders, current medications, etc. We  
210 used the 556 first recordings in this dataset from 248 subjects, 39 to 81 years of age (mean age  $60.29 \pm 8.62$ , 137 male /  
211 111 female). The C3 channel data was chosen for the purpose of this project.

212 **2.1.5 Muse's Sleep Dataset (MSD)**

213 Muse S is a wireless sleep EEG headband manufactured by InteraXon (Toronto, ON, Canada). The data is sampled  
214 at 256 Hz, recorded from dry electrodes TP9, TP10, Fp1 and Fp2, and referenced at the FpZ electrode. We used 10  
215 recordings made between 2020 and 2022, provided by InteraXon, that were selected from Muse's Sleep Dataset (MSD).  
216 MSD is an internal dataset of overnight at-home sleep recordings collected with the Muse S EEG headset [52]. This  
217 dataset was collected in accordance with the privacy policy that users agree to when using the Muse headband and  
218 ensures their informed consent concerning the use of EEG data for scientific research purposes. The subjects were 26 to  
219 68 years old (mean age  $38.70 \pm 13.07$ , 7 male / 3 female) at the time of recordings. Sleep stages for these recordings  
220 were produced by Muse's proprietary automated sleep staging algorithm [52]. Due to the increased presence of artifacts  
221 in the data recorded from dry EEG electrodes [79], for each subject, we marked the 30s epochs with a standard deviation  
222 larger than that of the whole recording, thus dropping an approximate 7.48% of all epochs from power spectral analysis  
223 & model fitting across the entire dataset. In this work, we use the EEG data in the TP7 channel from the MSD dataset,  
224 as it uses a frontal reference, thus quantifying the differential trace between the temporoparietal and frontal electrodes.

Table 1: Abbreviations and descriptions of sleep the hypnogram-based sleep metrics calculated using YASA

Metric	Description	Unit
TIB	Total duration of the hypnogram.	min
SPT	Total duration from first to last period of sleep.	min
WASO	Duration of wake periods between the first and last periods of sleep	min
TST	Total duration of N1 + N2 + N3 + REM sleep between the first and last periods of sleep.	min
SE	$(TST / TIB) \times 100$	%
SME	$(TST / SPT) \times 100$	%
SOL	Latency to first epoch of sleep	min
$<Stage>$ Latency	Latency to the first instance of the sleep stage $<Stage>$	min

225 We also obtained a second set of 78 EEG recordings from 2 Muse S users, to use as a case study examining the suitability  
226 of such repeated nightly EEG recordings for monitoring sleep health and brain activity. These 2 users recorded their  
227 sleep at least every other night for a total period of 30-60 days. User 1 has 32 recordings and user 2 has 46 recordings.  
228 All processing steps were done similar to the MSD data described above. These 78 recordings were not used for the  
229 general group-level analyses, as they include a mix of normal and abnormal sleep parameters across various nights.

## 230 2.2 EEG & Hypnogram Data Analysis

### 231 2.2.1 Pre-processing

232 The data were organized and processed using MNE-Python [80]. The power spectral density from the data was  
233 calculated in 30s segments using Welch's method [81] in 4s Hamming windows with a 1s overlap. Choice of window  
234 lengths in EEG signal processing should be optimized for the analysis objectives in question [82]. In the present case,  
235 this choice of window sizes was made to balance the sharpness of the peak frequencies –due to noise-driven changes in  
236 the power of those bands– with a physiologically-plausible level of specificity in key rhythms such as alpha (7.5-12 Hz).  
237 And the segment length here was chosen as it is the segment length over which the sleep stages are labelled. The sleep  
238 staging system used here is the 2007 standard, issued by the American Academy of Sleep Medicine (AASM) [12]. The  
239 epochs with stages marked as *unknown* were omitted for all datasets.

### 240 2.2.2 Aperiodic component estimation using FOOOF

241 We used the Python library FOOOF v1.0.0 to separate the periodic and aperiodic components of the empirical and  
242 fitted power spectra [83]. The algorithm fit a Gaussian power spectrum corresponding to the aperiodic component to  
243 each EEG PSD without a knee, in the range of 0-45 Hz, with bins of the size 0.25 Hz. The Gaussian spectrum was  
244 then deducted from the EEG power spectrum to separate the periodic (oscillatory) components. This process was  
245 implemented iteratively and optimized to get maximum 4 oscillatory peaks, each between 1 to 4 Hz in bandwidth, and  
246 with at least  $1 \text{ V}^2 / \text{Hz}$  amplitude. We used the extracted exponent (slope) & offset of the fitted aperiodic ( $1/f$ -like)  
247 component and the frequency & power of the periodic components to study the phenomenological properties of the  
248 power spectra.

249 **2.2.3 Calculating sleep metrics and statistics using YASA**

250 We used the Python library YASA v0.6.3 to estimate some common sleep metrics based on the presented hypnograms  
251 [84]. This library calculated values for sleep architecture and quality metrics using the subjects' hypnograms according  
252 to the AASM guidelines [12]. Table 1 includes these evaluated metrics.

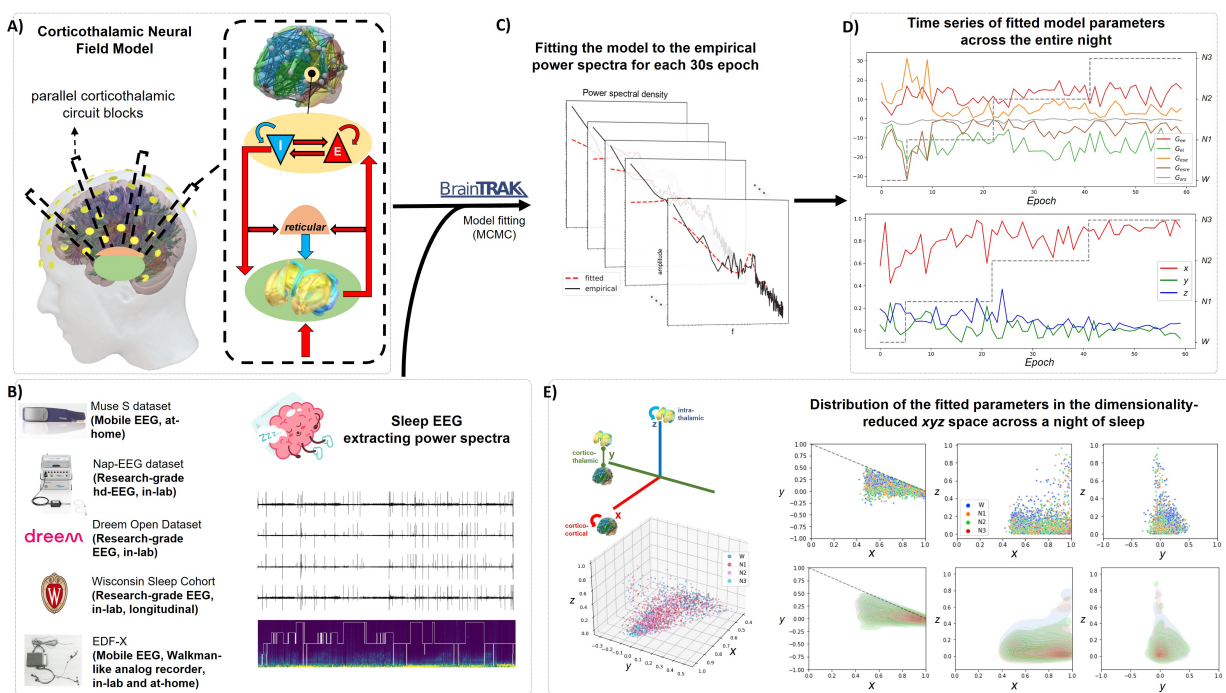


Figure 1: **Method for fitting the sleep EEG power spectra to the model.** **A)** Schematic of the neurophysiological model of the thalamocortical system, which simulates each channel of EEG as an independent active unit spanning the thalamic and cortical components. **B)** With this in mind, we accessed 5 datasets (EDF-X, Nap-EEG, DOD, WSC, MSD) which included sleep EEG and hypnograms. **C)** The *empirical* power spectra over 30-second epochs calculated using Welch's method and the *fitted* power spectra generated using Braintrak to yield the fitted parameters. **D)** Time series of the fitted gain ( $G$ ) parameters for subject 11, recording no. 1, from the Nap-EEG dataset. Each fitted epoch yields a set of 5 gains. The gain parameters are then used to calculate the circuit gain parameters  $x, y, z$ . **E)** Distribution of the parameters  $x, y, z$  across the entire Nap-EEG dataset is shown. Different sleep stages are denoted by the colour of the dots in the scatter plot. Different stages are clustered in different areas of the subspace. The dashed line in the 2D  $x, y$  plot marks the stability boundary at  $x + y = 1$ .

253 **2.3 Neurophysiological Model of Thalamocortical Activity**

254 This work used a *neural field model* of thalamocortical dynamics to simulate plausible activity observed in the EEG data  
255 [30, 45]. In this physiological wave equation model, we model activity across these units of the thalamocortical circuitry,  
256 generated by: cortical excitatory (pyramidal) neurons ( $e$ ), cortical inhibitory interneurons ( $i$ ), thalamic reticular nucleus  
257 ( $r$ ) and thalamic relay nuclei ( $s$ ).

258 In each of these populations, a mean firing rate (i.e., pulse density) of each population denoted as  $Q_a$  is calculated based  
259 on the mean somatic voltage ( $V_a$ ). Henceforth in this document,  $a$  &  $b$  will represent any of the modelled populations,  
260  $a, b \in \{e, i, r, s\}$ .

261 With  $\theta_a$  as the mean firing threshold and  $\sigma'_a$  as the standard deviation of the somatic voltage for the population  $a$ , we  
262 can calculate  $Q_a$  as:

$$Q_a = S(V_a) = \frac{Q_a^{max}}{1 + e^{-\frac{(V_a - \theta_a)}{\sigma'_a}}}. \quad (1)$$

263 Using  $Q$ , the number of outgoing axonal spikes from the population ( $\phi_a$ ) can be determined via this equation:

$$D_a \phi_a = Q_a \quad (2)$$

264

$$D_a = \frac{1}{\gamma_a^2} \frac{\partial^2}{\partial t^2} + \frac{2}{\gamma_a} \frac{\partial}{\partial t} + 1 - r_a^2 \nabla^2, \quad (3)$$

265 where  $D_a$  is a nonlinear term that dampens the incoming spike rate into a *field* equation ( $\phi$ ), and the temporal damping  
266 rate is  $\gamma_a = v_a/r_a$ . For each population  $a$ ,  $v_a$  is the axonal conduction velocity, which is approximated to 10 m/s  
267 for myelinated axons that form the thalamocortical projections.  $r_a$  is the total range of axons of type  $a$ . This model  
268 assumes that long-range connections are myelinated and hence have a higher  $v_a$ . Shorter-range connections are not  
269 myelinated and will only have negligible values, of  $v$ , rendering their effects on cortical activity insignificant. Among  
270 the thalamocortical connections, only the thalamic relay-excitatory cortical ( $r \leftrightarrow e$ ) connection has a non-negligible  
271 distance, and as a result, we can take  $r_e$  as the only significant  $r$  value affecting the propagation and assume the other  $r$   
272 values to be 1.

273 In the subcortical units ( $r$  and  $s$ ), we also assume spatial uniformity such that  $\nabla^2 = 0$ . Given the large value of  $\gamma_a$   
274 for the thalamocortical connection, the damper term ( $D_a$ ) converges to 1. As such, we can approximate that in the  
275 physiological states,  $Q_a = \phi_a$ .

276 To account for the delays introduced by the synapses, we introduce  $1/\beta$  and  $1/\alpha$  which are respectively the *rise* and  
277 *decay* time constants of the postsynaptic soma activation, in the response of a population to a spike. We can write the  
278 dendritic impulse response function as:

$$L(u) = \frac{\alpha\beta}{\beta - \alpha} (e^{-\alpha u} - e^{-\beta u}) \quad (4)$$

279 So, if  $\alpha \neq \beta$ , the dendritic activation function can be written as:

$$D_{\alpha\beta} = \frac{1}{\alpha\beta} \frac{d^2}{dt^2} + \left( \frac{1}{\alpha} + \frac{1}{\beta} \right) \frac{d}{dt} + 1 \quad (5)$$

280 The Fourier transform of  $L(u)$  yields a function in which the dendritic impulse response acts as a low-pass filter with  
281 the cut-off frequency at  $\alpha$ , and exhibiting a more steep attenuation at  $\beta$  Hz:

$$L(\omega) = (1 - \frac{i\omega}{\alpha})^{-1} (1 - \frac{i\omega}{\beta})^{-1}, \quad (6)$$

282 where  $\omega = 2\pi f$  is the angular frequency and  $f$  is the frequency in Hz.

283 We take  $V_a(r, t)$  to be the electrical field (voltage) in population  $a$ , influenced by: 1)  $\phi_{ab}$  which is the incoming  
284 activation by the presynaptic populations from population  $b$ , 2)  $N_{ab}$  the mean number of synapses between  $a$  and  $b$ , and  
285 3)  $s_{ab}$  the strength of each synapse between these two populations (the time-integrated response strength in the soma  
286 for each incoming spike):

$$V(r, t) = \sum_b V_{ab}(r, t) \quad (7)$$

287

$$D_\alpha(t) V_{ab}(r, t) = N_{ab} s_{ab} \phi_b(r, t - \tau_{ab}) \quad (8)$$

288 We further define  $\nu_{ab} = N_{ab} s_{ab}$  as the strength of all incoming synapses. The value of  $s$  (and hence  $\nu$ ) are considered  
289 positive for excitatory neurons and negative for inhibitory neurons. In this work, we assume *random connectivity* in  
290 the excitatory and inhibitory populations in the cortex, which means that  $N_{ia} = N_{ea}$  for any population  $a$ . Therefore,  
291 we simplify the  $\nu$  values as follows:  $\nu_{ee} = \nu_{ie}$ ,  $\nu_{ei} = \nu_{ii}$ , and  $\nu_{es} = \nu_{is}$ . Hence, we are left with the 8 independent  $\nu$   
292 values:  $\nu_{ee}$ ,  $\nu_{ei}$ ,  $\nu_{es}$ ,  $\nu_{se}$ ,  $\nu_{sr}$ ,  $\nu_{rs}$ ,  $\nu_{re}$ , and  $\nu_{sn}$ .

293 By taking the Fourier transform of Eqn. (8), we can represent the cortical excitatory field ( $\phi_e$ ) in terms of the external  
294 sensory input field ( $\phi_n$ ) in the Fourier domain:

$$\frac{\phi_e(k, \omega)}{\phi_n(k, \omega)} = \frac{G_{es} G_{sn} L^2 e^{i\omega t_0/2}}{(1 - G_{srs} L^2)(1 - G_{ei} L)(k^2 r_e^2 + q^2 r_e^2)} \quad (9)$$

$$q^2(\omega) r_e^2 = \left(1 - \frac{i\omega}{\gamma_e}\right)^2 - \frac{G_{ee} L(\omega) + G_{es} L(\omega) S}{1 - G_{ei} L(\omega)}, \quad (10)$$

(11)

$$S = \frac{(L G_{se} + L G_{sr} L G_{re}) e^{i\omega t_0/2}}{1 - L G_{sr} L G_{rs}}, \quad (12)$$

295 where  $k = 2\pi/\lambda$  is the wave vector with wavelength  $\lambda$ .

296 In a steady state, can assume  $V_a$  to be the only the perturbations to the function and take a linearized approximation of  
297 Eqn. (1), around the first term of the Taylor expansion. We define the parameter  $\rho$  as the derivative of the first term in  
298 this expansion. Hence we can reinterpret Eqn. (1) as:

$$Q_a(r, t) = \rho_a V_a(r, t) \quad (13)$$

$$\rho_a = S'(V_a^{(0)}) \quad (14)$$

299  $G_{ab}$  is defined as the gain value between populations  $a$  and  $b$ , describing the strength of the response in population  
300  $a$  as the result of the unit input of population  $b$ , determined by all the scalars that affect the activation of a synaptic  
301 population:

$$G_{ab} = \rho_a \nu_{ab} = \rho_a N_{ab} s_{ab} \quad (15)$$

302 These gain variables are multiplicative, so that  $G_{abc} = G_{ab}G_{bc}$ . In this manner, the gains in functionally significant  
303 loops can be simplified as  $G_{ese} = G_{es}G_{se}$  representing the excitatory cortico-thalamo-cortical loop directed by the  
304 thalamic relay nuclei,  $G_{esre} = G_{es}G_{sr}G_{re}$  representing the inhibitory cortico-thalamo-cortical loop directed by both  
305 the thalamic relay and reticular nuclei, and  $G_{srs} = G_{sr}G_{rs}$  representing the gain in the inhibitory intrathalamic  
306 feedback loop.

307 In this case, we assume the uniform distribution of the cortical excitatory units (that is, spatially-uniform values of  
308 the wave vector  $k$ ). If we approximate the brain as a finite-sized rectangular sheet with dimensions  $lx \times ly$ , we can  
309 calculate the EEG power spectrum  $P(\omega)$  as the integration of  $\phi_e(k, \omega)$  over the wave vector  $k$ :

$$P_{EEG}(\omega) = P_0 \left| \frac{L(\omega)T/G_{sn}}{1 - G_{ie}L(\omega)} \right|^2 \frac{(2\pi)^2}{lx ly} \times \sum_{m,n=-\infty}^{\infty} \frac{e^{-k_{m,n}^2 k_0^2}}{|k_{m,n}^2 r_e^2 + q^2(\omega) r_e^2|^2}, \quad (16)$$

310 where:

$$T = \frac{LG_{sn} e^{i\omega t_0/2}}{1 - LG_{sr} LG_{rs}}, \quad (17)$$

$$P_0 = \frac{\pi |\phi_n|^2}{r_e^2} G_{es} G_{sn} \quad (18)$$

$$k_{m,n}^2 r_e^2 = (2\pi m r_e / l_x)^2 + (2\pi n r_e / l_y)^2 \quad (19)$$

311 In Eqn. (16), the term  $e^{-k_{m,n}^2 k_0^2}$  represents the low-pass spatial filtering induced by the dispersion of EEG electrical  
312 fields through the scalp and the cerebrospinal fluid between the cortex and the EEG sensor. This dispersion will also be  
313 spatially uniform given the uniformity of the vector  $k$ . The low-pass cutoff  $k_0$  is set at  $10 \text{ m}^{-1}$  based on prior empirical  
314 observations by Srinivasan et al. [85].

315 To mitigate the effects of high-frequency EMG artifacts introduced by pericranial, cervical, and extraocular muscles on  
316 the higher frequencies in of the power spectra [86, 87], an additional EMG power spectrum is added to that of the EEG  
317 [88, 89]:

$$P_{total}(\omega) = P_{EEG}(\omega) + A_{EMG} \left( \frac{\omega / 2\pi f_{EMG}}{1 + (\omega / 2\pi f_{EMG})} \right)^2, \quad (20)$$

318 where the  $A_{EMG}$  term is fitted together with the other parameters for  $f_{EMG}$  in the range of 10 to 50 Hz.

319 It is worth noting regarding Eqn. (16) that by fitting this power spectrum function, we only get 5 gain ( $G$ ) values ( $G_{ee}$ ,  
320  $G_{ei}$ ,  $G_{ese}$ ,  $G_{esre}$ ,  $G_{srs}$ ) along with  $\alpha$ ,  $\beta$ ,  $t_0$ , and the fitted artifact term  $A_{EMG}$ . There are infinite solutions to find  $\nu_a$   
321 with the power spectrum model fitting approach, since  $\nu_a = N_a s_a$ . Similar to  $\nu$ , the values of the gain parameters are  
322 negative for inhibitory synapses and positive for excitatory synapses, making  $G_{ei}$  and  $G_{sr}$  negative and all the other  
323 gains positive.

324 **2.3.1 xyz space**

325 In the stable regions of the 9-dimensional parameter space at low frequencies, a reduced 3-dimensional space could be  
326 defined to represent the model parameters, in which: 1)  $x$  is the cortical loop gain and represents the corticocortical  
327 connection strength, 2)  $y$  is the corticothalamic gain and represents how effectively the thalamus can drive cortical  
328 activity, and 3)  $z$  is the intrathalamic gain. These three parameters are calculated via the following equations:

$$x = \frac{G_{ee}}{(1 - G_{ei})} \quad (21)$$

$$y = \frac{G_{ese} + G_{esre}}{(1 - G_{srs})(1 - G_{ei})} \quad (22)$$

$$z = \frac{-G_{srs}\alpha\beta}{(\alpha + \beta)^2} \quad (23)$$

329 Each underlying state of brain activity gives more or less unique combinations of  $xyz$ . This system can be used to  
330 represent thalamocortical activity in many brain states with fewer dimensions than the entire fitted parameter set.  
331 Eqn (22) asserts that the balance between cortical excitatory versus inhibitory activity determines the positive or negative  
332 sign of  $y$ . Excitation brings  $y$  toward more positive values, and inhibition will shift it to negative values. Eqns (21) and  
333 (23), respectively, indicate that the values of  $x$  and  $z$  will always be positive.

334 **2.4 Simulation and model fitting**

335 Simulations and model fitting were performed in MATLAB using the *Braintrak* library [89, 51, 90]. This toolbox  
336 implements a Markov Chain Monte Carlo (MCMC) method, using the Metropolis-Hastings algorithm for model fitting.  
337 The analytic power spectrum of the model, as defined in Eqns. (16) & 20, was fitted to the empirical power spectra  
338 from 30-second windows in the data. The parameters implemented were restricted to the stability limits defined in the  
339 previous literature [51] to ensure the biological feasibility of the attained fitted parameters. Furthermore, the value of  
340 the gain parameters for all connections was limited to 20 ( $|G_{ab}| < 20$ ) to reduce the sensitivity of the model to noise in  
341 the input.

342 **2.4.1 Fitting metrics**

343 Using the method described above, we fitted the parameters of the corticothalamic model to empirical data. We used  
344 chi-squared ( $\chi^2$ ) error for model optimization, calculated between the 1 and 45 Hz frequency bins. The optimisation  
345 target function aims to reduce the error  $\chi^2$  between the empirical and model-generated power spectra. In this model  
346 fitting approach, the parameter space is firstly explored during a random walk with a length of 50,000 and with large  
347 step sizes, accepting the top points which get us to a region close to the target values. After this "burn-in" period,  
348 Braintrak takes smaller steps to approximate the ground truth more closely.

$$\chi^2 = \sum_j W_j \left| \frac{P_j^{exp} - P_j(x)}{P_j^{exp}} \right|, \quad (24)$$

349 where  $j$  corresponds to each unique Fourier transform frequency bin of the power spectra.  $P_j^{exp}$  is the empirical  
350 (experimental) power spectrum and  $P_j(x)$  is the predicted power spectrum for that bin. The term  $W_j$  is a scaling  
351 factor to increase the effect of the lower frequency bands compared to the higher frequency bands ( $W_j \propto f^{-1}$ ),  
352 thus increasing the sensitivity of the optimizer to the high frequency bins of the power spectrum and minimizing its  
353 sensitivity to lower frequencies. This can be valuable in reducing artifacts observed in the EEG data, since the main  
354 artifacts affecting our 1-45 Hz window include the glossokinetic, movement, eye blink, and sweat artifacts, all of which  
355 produce low-frequency artifacts that must be mitigated [91, 92].

356 The complexity of the model was also calculated using the Akaike Information Criterion (AIC) [93]. AIC denotes the  
357 complexity of the combinations of parameters that together yield the model power spectrum. The lower the value of  
358 AIC, the simpler (or more parsimonious) the model. High values of AIC may denote overfitting of power spectra by  
359 fitting complicated combinations of parameters. AIC is described by this formula:

$$AIC = 2k - 2 \ln(\mathcal{L}), \quad (25)$$

360 where  $k$  is the number of model parameters (9 in this case), and  $\mathcal{L}$  is the maximum of the likelihood function for this  
361 model.

362 **2.5 Correlations between model parameters and health parameters**

363 By fitting the described data to this model across many subjects and over several datasets, we will be able to investigate  
364 the correlations between the changes in the model parameters and sleep stages, sleep quality metrics, and health markers  
365 that may have been collected from the subjects. For instance, the WSC dataset contains many such labels corresponding  
366 to many things such as the medications they were taking, their age, self-scoring surveys of depression and anxiety, and  
367 many markers of endocrine and metabolic health. We characterized the differences between subjects  
368 on or off certain medications, and the changes in the model parameters between sleep stages. We further tested the

369 existence of linear relationships between the changes in the model parameters and the health markers, using Pearson's  
370 test via SciPy [94]. We then used the Benjamini-Hochberg method for False Detection Rate (FDR) correction [95].

371 Finally, we explored the ability of our estimated neurophysiological circuit parameters to predict disease outcomes  
372 using ML-based biomarker stratification. To this end, we separated the data into training and test groups, using a linear  
373 kernel Support Vector Machine (SVM) to classify binary health markers from the mean or variance of the fitted model  
374 parameters. The train/test data separation, load balancing, and training and testing of the model was done using the  
375 Python scientific computing library `scikit-learn` v1.1.2 [96].

### 376 3 Results

377 Our analyses in this study evaluated the methodology for neurophysiological modelling-based brain state estimation  
378 described above [51, 89] across several datasets recorded from research-grade and consumer-grade devices. In the  
379 following, we first summarize several key characteristics of the sleep EEG and hypnogram data used, and then turn to  
380 our model fitting results and their physiological interpretation.

#### 381 3.1 Comparison of EEG features across sleep datasets

##### 382 3.1.1 Hypnogram-based sleep stage compositions

383 As can be seen in the group-averaged hypnogram summaries (Fig. 2E), sleep stages N1-N3 and W (wake) are well-  
384 sampled across all five of the studied datasets. REM sleep is also present in all datasets except Nap-EEG, since the  
385 30-minute recordings used in that study are much shorter than the average 80-100 minute mark at which the first episode  
386 of REM appears [97]. The other four datasets all include several dozen minutes of REM-labelled sleep periods on  
387 average, although for the EDF-X dataset the average percentage of time spent in REM across the subject group is only  
388 2.99% and the REM sleep latency (as seen in Fig. 2A), is unusually long (average of around 515 minutes).

#### 389 *Improved sleep quality with mobile EEG*

390 Sleep efficiency (SE, the percentage of time from the whole recording spent in sleep) between all datasets is comparable,  
391 averaging between 66.61% and 92.86% — although we note that for three of the five datasets, this value is below  
392 the recommended healthy range of 80-100% [98]. This value is the highest for the Muse S dataset with 92.86%.  
393 Sleep maintenance efficiency (SME, the percentage of time in sleep between the first and last stages of sleep) is also  
394 comparable for all datasets, with Nap-EEG performing the best among all (98.23%), and Muse S performing best for  
395 the whole-night recordings. For Muse S, this is most likely due to the improved comfort factor associated with the light  
396 and non-intrusive nature of mobile EEG headsets and the fact that the recordings are done at the subjects' home and in  
397 their familiar and comfortable beds. This interpretation is further corroborated by comparing the subject-averaged total  
398 minutes of "Wake After Sleep Onset (WASO)" between the different datasets. Muse S subjects spend an average of

399 20.50 minutes awake after sleep onset, which is also the lowest among the whole-night recordings, further demonstrating  
400 that the subjects have less interrupted sleep when using mobile EEG equipment. This value is comparable to the range  
401 of 54-88 minutes for the three research-grade whole-night recordings (DOD, EDF-X, and WSC). Subjects also fall  
402 asleep faster with Muse S (average of 11.30 minutes Sleep Latency) than all other whole-night recordings, with the  
403 exception of EDF-X, for which an accurate sleep latency could not be calculated (see Supplementary Material section  
404 3.1). Thus, mobile EEG can contain a more naturalistic and representative sample of physiological states and sleep  
405 stages in a full night of sleep than conventional research-grade EEG, and help us evaluate the normative trajectories of  
406 their changes in health and disease.

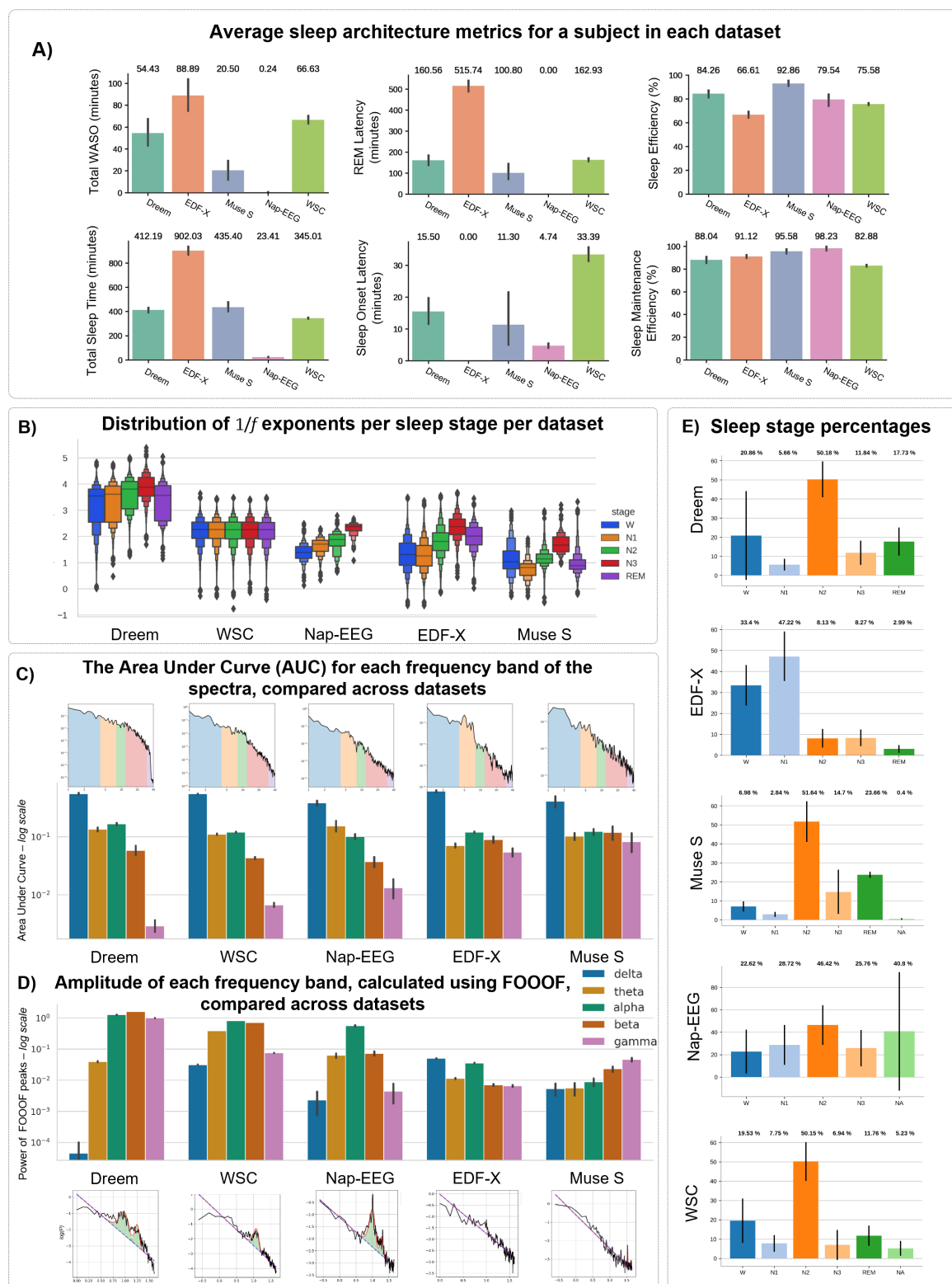


Figure 2: **Comparison of sleep architecture metrics and power spectral features across datasets.** A) Average metrics evaluating sleep architecture and sleep quality in a recording, compared across the datasets. Error bars represent the standard deviation of the values per subject. B) Distribution of  $1/f$  exponents in each dataset, separated across the various sleep stages. C) bottom: Subject-averaged area under curve (AUC) of the EEG spectral power for each frequency band. top: Example power spectra from the dataset noted in the bar plot, with each under-curve band highlighted. D) Subject-averaged FOOOF-calculated peak power for each frequency band. E) Composition of the sleep stages forming the hypnograms in each dataset.

407 **3.1.2 EEG power spectral features across sleep stages**

408 In the next stage, we used two different prevailing approaches for a quantitative comparison of the power spectra across  
409 datasets:

410 I) In one approach, the background scale-free  $1/f$  activity is separated from the oscillatory activity with defined  
411 frequencies, and then the properties of each periodic & aperiodic component is examined. We used the Python  
412 library FOOOF for this task, as described in section 2.2.2.

413 II) The second approach is to compare the areas under curve (AUC) for the power spectral plots in each of those  
414 frequency bands. We used the trapezoidal integration method to calculate the AUC.

415 ***Aperiodic components vary across datasets and track sleep stages robustly***

416 We separated the periodic and aperiodic components of the power spectra using FOOOF and calculated the exponent  
417 of the  $1/f$  component for each power spectrum. The range of the  $1/f$  exponents from different datasets are vastly  
418 different. Regardless of this variance, moving from lighter to deeper NREM sleep is generally associated with an  
419 increase in the value of the exponent and the value is then reduced again in the transition to REM sleep (Fig. 2A).

420 The scale-free changes in the slope of the  $1/f$  component, which are thought to be results of background physiological  
421 processes and general brain activity patterns [99] can disproportionately increase the AUC in low-frequency domains,  
422 including delta (slow) and sub-delta (infra-slow) frequencies. We see this by comparing the power of each band as  
423 compared using FOOOF vs. AUC methods in Fig 2: The datasets Dreem and WSC, which possess the highest average  
424  $1/f$  exponents (as noted in Fig. 2A) demonstrate highest AUCs in the delta band (Fig. 2B), but by using FOOOF to  
425 separate the periodic & aperiodic components and examine the height of each unique peak apart from the contributions  
426 of  $1/f$ , we observe that the delta band is the least dominant of all peaks 2C.

427 In fact, we see in that comparison that delta is the highest-powered band compared to all other bands in each dataset if  
428 we only use the AUCs, but separating the  $1/f$  component using FOOOF relegates the rank of the delta peaks amplitudes  
429 to the last place in all cases. We further note that if we rely only on the AUCs, the alpha peaks are either the highest or  
430 the second-highest calculated peaks in all datasets with the exception of the Muse S. This demonstrates the importance  
431 of the contributions of the aperiodic component to the power of each frequency band in the power spectra and how it  
432 affects the traditional AUC methods for calculating band power. Solely observing the AUCs for each of those bands  
433 without this separation would have concluded a domination of low-frequency activity for all datasets, with minimal  
434 difference across the datasets, but FOOOF allows us to make that distinction between the footprints of each recording  
435 setup on band peak amplitudes.

436 In the MSD data, the peak height is lower than the other datasets for most bands (Fig. 2C). Separating the  $1/f$   
437 components from the raw power spectra in for this dataset almost completely reverses the order of the peaks with  
438 regards to frequency: the  $1/f$ -separated peaks are highest for gamma and the lowest for delta, but the the AUCs are

439 highest for delta and lowest for gamma. This points to the fact that for this dataset, the  $1/f$  component is more dominant  
440 than the periodic component and that the  $1/f$  exponent is a robust feature separating the sleep stages and the  
441 physiological state of the subject, as evidenced by its strong variation across different sleep stages for Muse S (Fig. 2A),  
442 consistent with prior literature showing that most of the variation in individual sleep stages can be explained by  $1/f$   
443 components [36]. The  $1/f$  exponents are one of the canonical features of our physiological model's power spectra as  
444 well, as described in Robinson et al. [30], where the power law of the power spectra is a defining feature of the system,  
445 directly correlating with cortical gains and the primary oscillation frequencies, thus also making it a suitable criterion  
446 for tracking the activity of the corticothalamic circuitry.

447 **3.2 Physiological modelling**

448 Using the neurophysiological model of thalamic circuitry described in Abeysuriya et al. [51], Abeysuriya and Robinson  
449 [89], we fit the EEG power spectra across the various datasets. Despite the considerable difference in the properties of  
450 the EEG power spectra across these datasets, the model still performs well in fitting to all data. Goodness of fit was  
451 satisfactory, with all models demonstrating similar distributions of error ( $\chi^2$ ) and model complexity (AIC), meaning that  
452 the model is fitting closely to power spectra without over-complicating the model parameters. The error distribution is  
453 marginally higher for Dreem than for other datasets which could be explained by the wide distribution of  $1/f$  exponents  
454 in this dataset (Supplementary Fig. S1). The resulting fitted model parameters from all datasets exhibit patterns of  
455 change across sleep stages that are similar and in line with prior literature on thalamocortical communication in sleep.  
456 Corticothalamic communication is reduced in sleep and decreases further as the subject goes into deeper NREM sleep  
457 stages.

458 **3.2.1 Physiological transitions from light to deep NREM**

459 The regular progression of sleep stages throughout a night of sleep commences with wakefulness (W), then transitioning  
460 to light NREM sleep (N1), followed by deeper stages of sleep (N2 and N3), eventually reaching REM sleep. Each  
461 individual cycles through the REM/NREM stages multiple times, with the cycles taking an average of 90 minutes [97].  
462 In this transition within NREM sleep from N1 to N2 and to N3, the physiological properties of the functional brain  
463 circuits change along a clear trajectory [51], which we quantify using our neurophysiological modelling approach.

464 We first demonstrate this characteristic trajectory [51] and the differences between sleep stages using power spectra  
465 and fits from the Nap-EEG dataset. Similar overall results are obtained with the other four datasets, which are detailed  
466 further in the Supplementary Material Fig. S4. During the transition from W to N3, the  $1/f$  exponent becomes larger  
467 and peaks in the alpha frequency band are reduced as deeper stages are reached (Fig. 3A). Two major patterns are  
468 observed in the neurophysiological model in conjunction with this change in the power spectra:

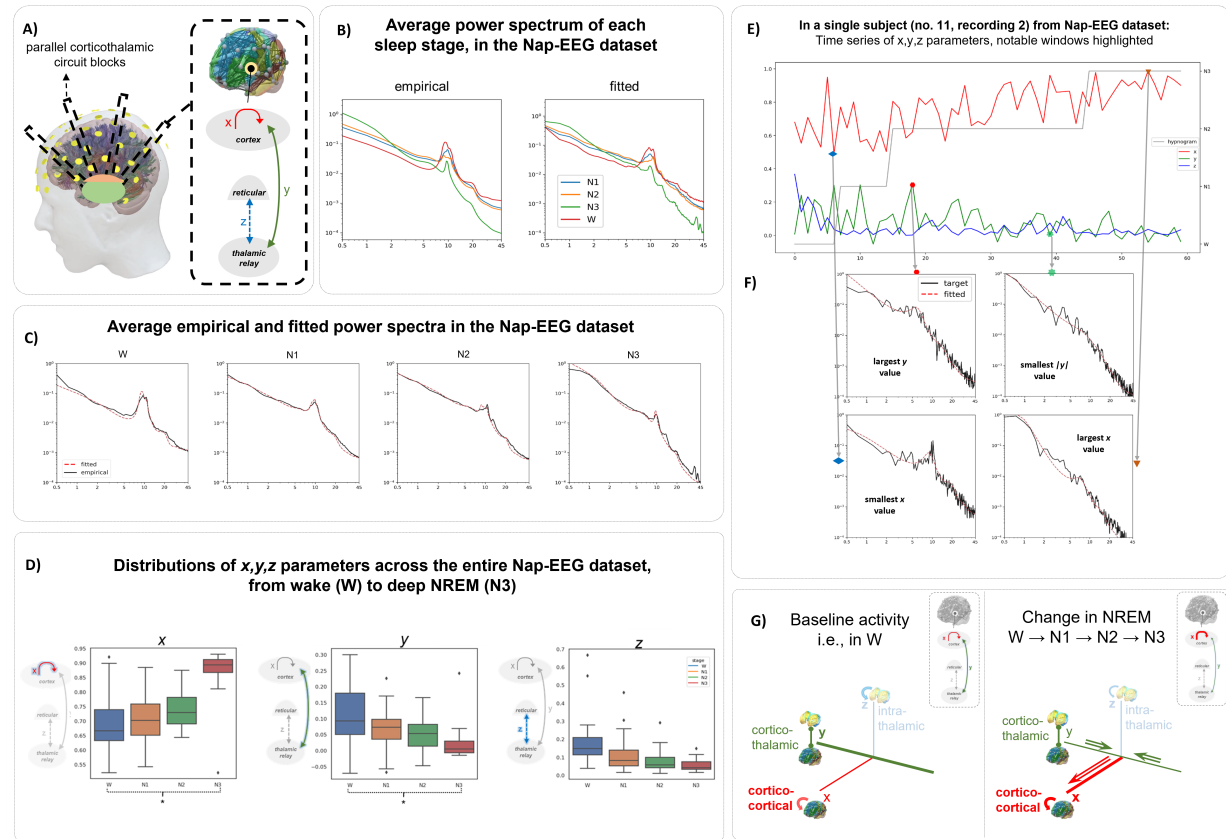


Figure 3: **Tracking the changes in the parameters in different sleep stages in the Nap-EEG dataset.** **A)** High-level schematic of the corticothalamic model, as described by the corticocortical ( $x$ ), corticothalamic ( $y$ ), and thalamocortical ( $z$ ) connection strengths. **B)** Average empirical vs. fitted spectra in the entire dataset, separated by sleep stages. **C)** Average power spectra in each sleep stage, separated between empirical and fitted. **D)** Box plots comparing the distribution of  $x$ ,  $y$ , and  $z$  parameters across different sleep stages. Stages with significant difference in mean parameters are denoted by (\*). **E)** Visualization of the  $xyz$  time series in conjunction with the hypnogram for one complete recording. **F)** Comparison of fitted and empirical power spectra at notable points in the whole-recording  $xyz$  time series with extreme  $x$  or  $y$  values, noting the associated alterations in the power spectra. **G)** Schematic demonstrating the change observed in the following panels. As the subject transitions from light to deep NREM, the connection strength in the corticocortical circuit is increased and the connection strength of the corticothalamic circuitry approaches zero.

#### 469 **Corticocortical amplification is increased from W to N3**

470 Figure 3C shows the distribution of the corticocortical ( $x$ ), corticothalamic ( $y$ ), and intrathalamic ( $z$ ) loop gain  
 471 parameters across all epochs in the Nap-EEG dataset. The parameter  $x$ , calculated according to Eqn. 21, represents the  
 472 net corticocortical excitatory connection strength. This parameter takes values between 0 and 1, with values close to 1  
 473 demonstrating highest degree of excitatory corticocortical amplification via the excitatory projections connecting  
 474 the various cortical regions and lowest corticocortical inhibition.

475 As can be seen, the progression from lighter to deeper sleep stages (N1 → N2 → N3) is associated with an increase in  
 476 the average value of  $x$ , with estimates of this parameter in N3 approaching its maximum value of 1. This observation  
 477 was confirmed statistically with an independent-samples  $t$ -test, which showed a significant increase in  $x$  from W to  
 478 N3 ( $t = 17.29, p < 0.001$ ). The corresponding comparison was also statistically significant in the other four datasets

479 (Supplementary Fig. S4). This points to an association between deep NREM sleep and reduced thalamocortical drive of  
480 cortical dynamics. The reduction in the absolute value means that the bottom-up thalamocortical drive, in either the  
481 inhibitory or excitatory modes, is reduced in NREM sleep.

482 ***Bottom-up thalamocortical modulation is reduced from W to N3***

483 During the transition from lighter to deeper stages of NREM, the distribution of  $y$  parameters—which indicates how  
484 strongly the thalamus drives cortical dynamics via thalamocortical projections—becomes narrower and more leptokurtic,  
485 with the absolute value of  $y$  decreasing and approaching 0. Based on the properties of the  $y$  circuit parameter, this  
486 signifies a reduction in the influence of thalamocortical gains (both inhibitory or excitatory). Per Eqn (22), positive  
487 values of  $y$  would denote the dominance of the excitatory part of the corticothalamic loop ( $G_{ese}$ ) over the inhibitory part  
488 ( $G_{esre}$ ), and hence net excitatory bottom-up stimulation thalamo-cortically. In contrast, negative values of  $y$  signify the  
489 dominance of the term  $G_{esre}$ , where the inhibitory effect is due to GABAergic projections from the thalamic reticular  
490 nucleus. The negative value  $y$  therefore denotes a net inhibition applied to the cortex by the thalamus. As can be  
491 seen in the middle panel of Figure 3C the absolute value of  $y$  in N3 sleep approaches 0, signifying the absence of  
492 excitation or inhibition driven from the thalamus towards the cortex. Similarly to the previous section, we used the  
493 independent-samples  $t$ -test to compare the  $|y|$  values between stages W and N3, demonstrating a significant reduction in  
494 the parameter ( $t = -11.48, p < 0.001$ ). Again, this effect was replicated across the other four datasets (Supplementary  
495 Fig. S4).

496 To further confirm that this relationship constitutes an ordinal trend across all four sleep stages, we assigned NREM  
497 sleep depth values of 0-3 to stages W-N3, and performed Pearson's  $r$ -test with these and the lumped circuit gain  
498 parameters. This returned significant correlations between sleep depth and both the absolute corticothalamic circuit  
499 gain  $|y|$  ( $r = -0.226, p < 0.001$ ) and corticocortical circuit gain  $x$  ( $r = 0.301, p = 9.83 \times 10^{-45}$ ).

500 **3.2.2 Relationship of physiological circuit parameters to periodic and aperiodic EEG power spectrum features**

501 We have demonstrated physiological model-based extraction of information on corticothalamic system state from  
502 windowed EEG power spectra across sleep stages and in multiple datasets. A key question that this analysis raises is  
503 "what features of the computed spectra contribute to the estimated physiological parameters"? As noted in Figure 2,  
504 different sleep stages have characteristic fingerprints across the periodic and aperiodic ( $1/f$ ) components of the EEG  
505 power spectrum, that are generally consistent across all five datasets studied here. Given the evident associations of  
506 each sleep stages with the corticothalamic circuit activity parameters (Fig. 3) as well as the aperiodic components of the  
507 power spectra (Fig. 2A), we aimed to directly determine the interplay between the strength of various thalamocortical  
508 sub-circuits (gain ( $G$ ) parameters) and the broadband power and  $1/f$  exponents of the power spectra, along with a  
509 comparison of how each of these parameters relate to the changes in the power spectra.

510 To determine more precisely how the aperiodic components of the empirical power spectra give rise to the fitted  
511 physiological model parameters, we studied the correlation of these parameters across the entire Nap-EEG dataset  
512 with the slope and offset of the  $1/f$  (Fig. 4A). This step was repeated for all datasets and all gain parameters in the  
513 Supplementary Figs. S5 – S9. We then examined further the contributions of isolated individual parameters to the  
514 power spectrum structure, by first initializing models at the estimated parameter values from a typical fitted epoch, and  
515 then systematically manipulating each gain ( $G$ ) parameter, per Eqns. (16) –(19), observing changes in the model power  
516 spectra (Fig. 4B).

517 ***Lower thalamic and corticothalamic gains generate a steeper  $1/f$***

518 In all datasets,  $G_{ese}$ —the circuit gain related to the positive feedback loop between the cortex and the thalamic relay  
519 nuclei—has a significant negative correlation with the exponent and the offset of the  $1/f$  component (Figure 4A). That  
520 is, stronger excitatory corticothalamic feedback, signified by a higher  $G_{ese}$ , results in a flatter  $1/f$  component and a  
521 reduced area under the curve in the low-frequency domain. In general, we observe in the model fit results that epochs  
522 from sleep stage N3 tend to cluster in regions of parameter space with lower  $G_{ese}$  values and higher  $1/f$  exponents.  
523 Thus, through the progression from wake to light and into deeper sleep, the exponent of the  $1/f$  components increases,  
524 due to the progressive weakening of the excitatory corticothalamic feedback loop, as predicted analytically in Robinson  
525 et al. [30]. Concurrently with this, a positive correlation is observed between  $1/f$  exponents and the negative-valued  
526 (inhibitory) gains of the loops associated with the thalamic reticular nucleus ( $G_{esre}$  and  $G_{srs}$ ). As can be seen clearly  
527 in Figure 4B), a decrease in the  $1/f$  exponent and offset (flatter aperiodic component) is observed as both of these  
528 negative inhibitory gains become more pronounced. This is in line with observations by Abeysuriya et al. [51], in which  
529 a significant reduction in the strength of thalamothalamic inhibitory connections—represented by thalamo-thalamic  
530 circuit gain ( $z$ )—was observed in deeper sleep stages, which possess power spectra with higher  $1/f$  exponents (Fig. 2A).

531 ***Greater corticocortical excitation can yield steeper  $1/f$  components***

532 The analyses in Figure 4B also show that amplifying the gains in the cortical excitatory ( $G_{ee}$ ) or inhibitory ( $G_{ei}$ )  
533 connections results in a broadband increase in spectral power. The increase in  $G_{ee}$  is slightly more effective at increasing  
534 the lower frequency components. However, unlike the effects noted above for  $G_{ese}$ ,  $G_{esre}$  and  $G_{srs}$ , modulation of  
535  $G_{ee}$  or  $G_{ei}$  was not found to influence the observed spectra in this way in the datasets studied, and the correlations  
536 between these gain parameters and the  $1/f$  components are not strongly correlated (Supplementary Fig. S7).

537 To further evaluate this effect of the gains on  $1/f$  exponents, the analysis above was conducted for all the other datasets  
538 in addition to Nap-EEG (Supplementary Figs. S5–S9) which confirms this effect for most of the datasets. All of the  
539 datasets, with the exception of WSC, demonstrate significant moderate correlations between  $1/f$  exponents and the  
540 corticothalamic gains ( $G_{ese}$  and  $G_{esre}$ ) and insignificant or significant mild correlations between cortical gains and the  
541  $1/f$  exponents. Abeysuriya et al. [51] report  $G_{ee}$  to highest variability amongst the gain parameters between different  
542 sleep stages. Our findings demonstrate that this is not mediated by the  $1/f$  exponents at least in these datasets. In the

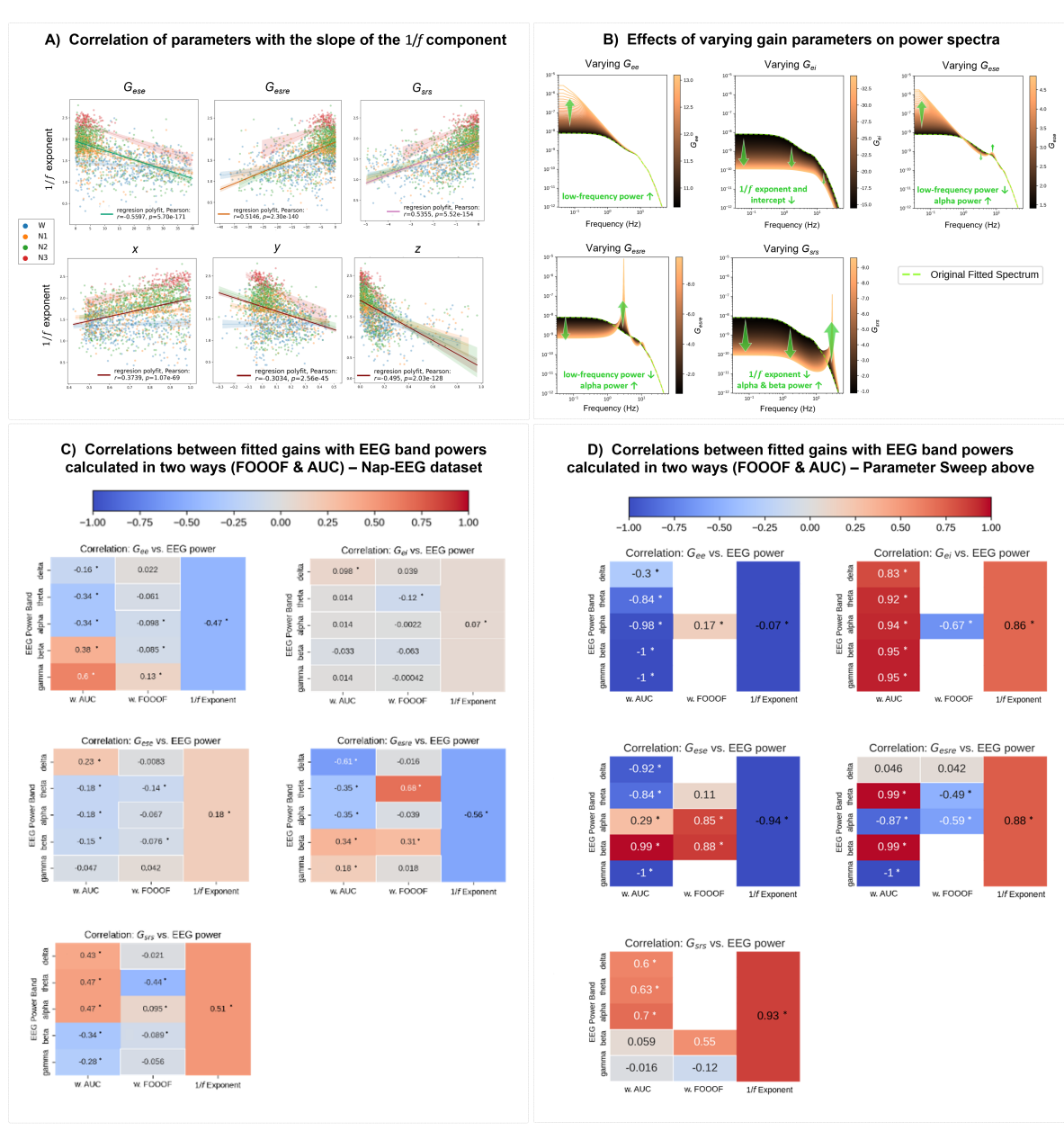


**Figure 4: Correlation between model parameters and the shape of the power spectra.** **A)** The correlation between the exponent of the aperiodic component with each thalamic gain parameter and  $x, y, z$ , calculated using Pearson's  $r$ -test.  $p$ - and  $r$ -values reported in each legend. **B)** The effects of the incremental increase of each gain parameter on the shape of the power spectra. The baseline power spectra (in black) was taken from the fit to a real 30-second epoch (in Nap-EEG in stage N2 with no prominent peak). The absolute value of each gain value was increased in steps of 0.05 and the power spectrum generated from those parameters was generated (deducting 0.05 from negative gains and adding 0.05 to negative gains in each step. The colour bar denotes the values specified, starting from the darker color as the baseline and changing the gain parameters successively towards the lighter copper colour. **C)** Correlation of the gain parameters with the EEG Band power and the  $1/f$  exponent in the Nap-EEG dataset **D)** Correlation of the gains with the power spectra resulting from the incremental sweep of the gain parameters.

543 case of WSC, the distribution of the  $1/f$  exponents does not differ greatly between sleep stages as seen in Fig. 2A,  
544 which suggests that it might not be as adequate an indicator of the brain's physiological state as it is for other datasets.

545 ***Fitted model parameters represent the power spectra robustly***

546 In the next step, we examined the correlations between the fitted gain parameters and the power of each band and  
547 the  $1/f$  exponent in the EEG power spectra, for each dataset and for the power spectra attained through the manual  
548 modification of single connection strengths. Pearson's  $r$ -tests were implemented between the power of each band for  
549 each power spectrum and the gain parameters corresponding to it. The statistical significance of each correlation was  
550 corrected for the repeated hypothesis testing using the Bonferroni method [100] to prevent the false detection of patterns.

551 It is observed that the offset & the exponents of the aperiodic components correlate with fitted parameters in the same  
552 direction and with similar strengths, as evidenced by Figs. S5 to S9. This analysis was completed for the Nap-EEG  
553 dataset in Fig. 3C and was repeated for all other datasets and all fitted and calculated parameters in the Supplementary  
554 Material Figs. S10 to S14.

555 It is notable that the gain parameters  $G_{ee}$  and  $G_{ese}$  are excitatory and hence have a positive sign. Meanwhile, the gains  
556  $G_{ei}$ ,  $G_{esre}$ , and  $G_{srs}$  are negative, and hence have a negative sign. Stronger connection strengths correspond to larger  
557 absolute values of these gains (more positive for the excitatory and more negative for the inhibitory). This must be  
558 taken into account when interpreting the correlations in Fig. 4.

559 Comparing the correlations for the fitted parameters (Fig. 4C) and the power spectra generated by changing the  
560 parameters (Fig. 4D) reveals that the positive gains are correlated and the negative gains are anti-correlated with the  
561 exponent of the  $1/f$  component. The direction of the correlations is similar for both instances (the sign of the  $r$ -value).  
562 However, the intensity of the correlations ( $|r|$ ) is larger for the manually-set parameters, which could be explained  
563 by the fact that all model parameters can also change for the fitted parameters, while in the manually-set instance,  
564 all parameters are fixed other than the changed parameter. The correlations between the changed parameter and the  
565 exponent in the set parameter instance is very strong ( $|r| > 0.86$ ) for all parameters except for that of the cortical  
566 excitatory self-connection ( $G_{ee}$ ). Examining the parameters fitted to the Nap-EEG dataset, those correlations are  
567 moderate ( $0.5 < r < 0.6$ ) for all parameters except for the cortical excitatory connection strength ( $G_{ee}$ ) and also the  
568 cortical inhibitory connection strength ( $G_{ei}$ ).

569 ***Physiological model captures changes in the spectra driven by both aperiodic and periodic components***

570 As seen in Fig 4D, in examples such as the direct modification of the cortical inhibitory connection strength ( $G_{ei}$ ) alone,  
571 we observe a very strong correlation of the gain with the EEG band power calculated via the "area under curve" (AUC)  
572 method. But by separating the periodic and aperiodic components using FOOOF, we observe a different phenomenon;  
573 the aperiodic ( $1/f$ ) exponent is increased in the same direction and approximately with the same intensity as the AUC  
574 band powers, but we only see one correlation with the FOOOF-discerned peaks in the alpha band, and no peaks were  
575 generated in any of the other EEG frequency bands. The case for the cortical excitatory connection strength ( $G_{ee}$ ) is  
576 somewhat different, where the AUCs of almost all bands except for delta have a very strong anti-correlation with the  
577 gain values ( $r > 0.84$ ), but the FOOOF-discerned  $1/f$  exponent does not show a notable correlation ( $r = 0.07$ ) and the  
578 only correlating FOOOF-detected peak is alpha, with a weak correlation ( $r = 0.17$ ).

579 As seen in Fig 4C, Comparing the FOOOF and AUC-detected phenomena in the parameters fitted to the Nap-EEG  
580 dataset demonstrates this common thread as well; all the connection strengths involving thalamus ( $G_{ese}$ ,  $G_{esre}$ , and  
581  $G_{srs}$ ) exhibit weak to moderate correlations with the AUCs of EEG bands, and they similarly correlate moderately with  
582 the  $1/f$  exponents. Comparing the  $r$ -values of the correlations between FOOOF and AUC-measured peaks with these  
583 three gains demonstrates a strong disagreement between these two common metrics of power band estimation, where  
584 only two of the peaks are strongly detected by both methods, and in the case of theta band activity, they change in the  
585 opposite directions. This is due to the effects of the change in the  $1/f$  component, where the exponent of this aperiodic  
586 component is correlated with the area under the low-frequency bands (e.g., delta and theta), and anti-correlated with the  
587 high-frequency bands. In other words, the shape of the power spectra and how it follows power law can change the  
588 detected values for those power bands.

589 Despite the variations, several consistent phenomena can be identified that are associated with higher absolute values of  
590 any of the three thalamic gains ( $|G_{\{ese,esre,srs\}}|$ ):

- 591 • The  $1/f$  component is moderately decreased ( $-0.51 < r < -0.56$ ).
- 592 • The AUC for the delta, theta, and alpha bands is decreased with a weak-to-moderate correlation (respectively,  
593  $-0.43 < r < -0.61$ ,  $-0.18 < r < -0.35$ , and  $-0.18 < r < -0.47$ ).
- 594 • The AUC for beta and gamma band is weakly decreased (respectively,  $-0.34 < r < -0.38$ ,  $-0.18 < r <$   
595  $-0.28$ ).
- 596 • FOOOF peaks in theta are increased with a moderate correlation ( $-0.44 < r < -0.68$ ).

597 We observe that the gain parameters attained by fitting the power spectrum can strongly capture the changes in both  
598 the periodic and aperiodic components of the power spectra. This model can describe both the broadband changes in  
599 the power spectra as described by the AUC measurements and the  $1/f$  components, and the sharp peaks in narrower  
600 frequency bands, as measured via the FOOOF peaks. Among the fitted datasets, the  $1/f$  exponents and the changes  
601 in the AUCs tend to describe the fitted gain parameters better than the sharp FOOOF-detected peaks in most of the  
602 datasets, as evidenced by Figs. 4C & 4D, pointing to the power of this model of EEG power spectra to represent the  
603 different power spectral features arising from the physiological properties of canonical brain circuitry.

604 **3.3 Connecting the data-oriented and model-based observations for an interpretable understanding of sleep**  
605 **EEG**

606 Features of sleep EEG change through health & disease, and by treatment. Common observations of such changes  
607 are usually data-oriented and describe statistical patterns in the time, frequency, phase, and spatial domains. Having  
608 described how the model tracks the periodic and aperiodic components of EEG power spectra, we now aim to see how  
609 these characteristics of the power spectra and their fitted model parameters map to various markers of sleep and mental  
610 health.

611 For that, we turn to two sources: **1)** The Muse S sleep EEG dataset includes repeated recordings from several users. We  
612 calculate key sleep quality scores from the hypnograms from these recordings to discern some nights with good or bad  
613 sleep quality. **2)** The Wisconsin Sleep Cohort dataset includes labels for many markers of physical and mental health,  
614 including medications taken by the participants.

615 We compare the power spectra and the fitted model parameters across different health states for the above two datasets  
616 to see find the changes associated with health, disease, and treatment.

617 **3.3.1 Observing changes in sleep EEG through repeated recordings using mobile EEG**

618 To demonstrate the utility of mobile EEG for continuous monitoring of sleep EEG in repeated nights, we analyzed a  
619 set of repeated sleep EEG recordings from two users, who conducted sleep EEG recordings at least every other day  
620 in a span of 30-60 days. Using the hypnograms, we calculated key sleep quality scores via the Python library YASA  
621 [84]. Each user has their consistent range of values for these sleep quality metrics which can be persistent over multiple  
622 nights. Looking at the trends of these parameters over time, we can find patterns pointing to changes in the sleep quality.

623 ***Each user has a unique subspace of model parameters***

624 repeated nightly recordings from the same user not only tell us about the night-by-night differences between their  
625 hypnograms, but also the large number of recordings allow us to characterize the subspace of parameters each individual  
626 will occupy in the available space of the model parameters. As we see in Fig. 5E, if we concatenate the parameters  
627 fitted to the epochs from all nights from each user, the general pattern of the inter-subject variability will start to be  
628 revealed. We can see that while the parameters of each sleep stage show great overlap especially around the mean  
629 values, the edges of these distributions are distinct, especially in wakefulness, N3, and REM. It is also worth noting  
630 that user 2 does not show N3 sleep in any of the nights. This shows the promise of mobile EEG for characterizing the  
631 normative sleep EEG of each individual based on their unique sleeping rhythm.

632 ***One user shows a trend of increasing REM percentage and N1/N2 latency across consecutive nights***

633 An interesting pattern that shows itself in the period of 30 recordings is that, as seen in Fig. 5, one participant (User 1)  
634 shows a trend of increasing REM percentage and increasing N1 & N2 latency over the observed period. Generally,  
635 such increase in the REM latency could be attributed to insomnia & sleep deprivation, or REM sleep disorders such as  
636 narcolepsy or REM sleep behavior disorder (RBD). But in the case of User 1, the Total Sleep Time (TST) is stable  
637 throughout the month, with the value of approximately 500 minutes, as are Sleep Efficiency (SE) & Sleep Maintenance  
638 Efficiency (SME) are also consistent, with respective ranges of 80-85 percent, and 80-90 percent. The REM latency for  
639 this user is fluctuating between 0 to 100 minutes, but this does not show a significant trend over time. This suggests that  
640 the increase in REM percentage is likely due to a disorder of REM sleep rather than a result of sleep deprivation or  
641 acute insomnia. In a systematic review, Boulos et al. [101] point to the parameter range of 8-21% for the average REM

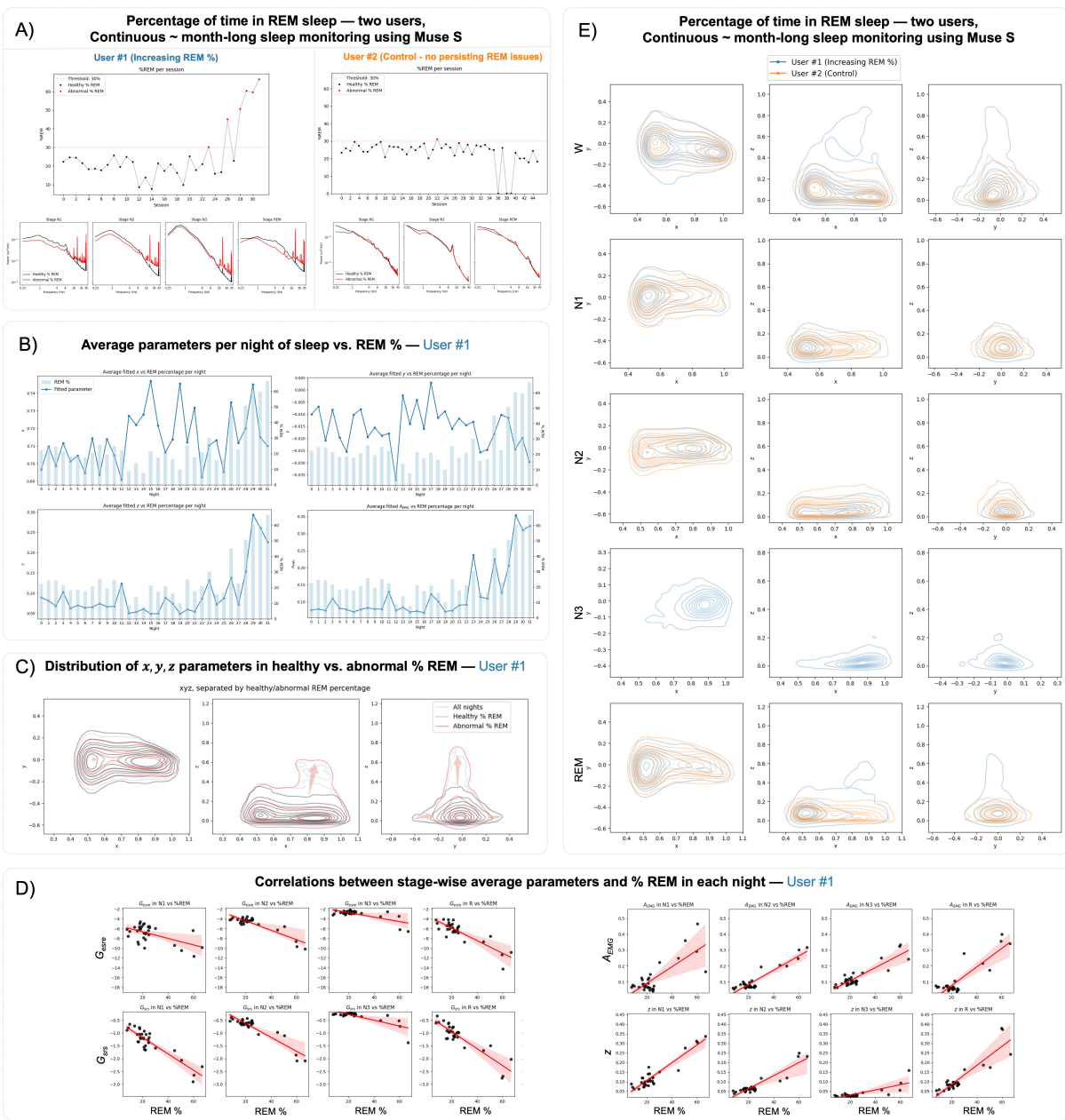


Figure 5: **Sleep quality metrics in repeated nights.** **A)** The percentage of time spent in REM sleep throughout the night for users 1 and 2 across the 30-60 day period. The stage-averaged power spectra are shown for nights with healthy vs. abnormal REM %. Values below 30% are considered normal in this case. **B)** Trends of the REM % (bars) vs. the trends of average  $x$ ,  $y$ ,  $z$  values (lines) for each recording, for user 1. **C)** The distribution of the  $x$ ,  $y$ ,  $z$  parameters across all epochs for healthy vs. abnormal REM % nights. Arrows point to the direction of the changes from healthy to unhealthy REM % nights. **D)** The average values of the thalamothalamic gain parameters for user 1, for nights with different REM % values. These trends are compared across sleep stages as well. **E)** The distribution of the  $x$ ,  $y$ ,  $z$  parameters across all nights for users 1 and 2.

percentage across the age groups between 18 and 81 years old. With that in mind, we designated a threshold of 30% to denote if the REM percentage is abnormally high. User 1 shows a trend of increasing REM percentage with consistent repetitive at-home recordings using mobile EEG. User 2 does not show a significantly high number of sessions with high REM percentage, though this user does not show N3 sleep in any of the sessions. These frequent recordings would

646 have been difficult and expensive to maintain over such a long period of time. This demonstrates a practical utility of  
647 mobile EEG for long-term monitoring of sleep EEG to find these potential patterns of sleep quality deterioration. In  
648 this section, we compare the power spectra and fitted model parameters across these two users and across the nights  
649 with good vs. excessive REM percentage, to delineate a difference in the data and how underlying mechanisms can  
650 underlie these differences.

651 ***Nights of sleep with high REM percentage have lower 1/f slopes and higher thalamo-thalamic inhibition***

652 In the next step, we compare the nights with high vs. low percentage of REM sleep. In figure 5A, we show that User 1  
653 has a clear trend of increasing REM % up to values of around 60%. In the first 20 recordings, this user has a range of  
654 REM % between 10 to 25 %, and this range increases night after night to approximately 70% in the 31st recording.  
655 User 2 does not show a significant trend of increasing REM % over time. To understand if there effects of the potential  
656 case of disordered REM sleep, we separated all the power spectra from all epochs of sleep from nights with *healthy* vs.  
657 *abnormal* (excessive) REM percentage and calculated the average spectra for each stage for both users.

658 We see in Fig. 5A that there are four clear changes in the power spectra from abnormal high-REM % nights compared  
659 to healthy REM % nights: 1) Descreasing 1/f slope (exponent) especially in N1 and REM. 2) Increased high-frequency  
660 power for all stages. 3) More prominent alpha peaks in N2, N3, and REM. 4) Increased high-frequency power ( 20  
661 Hz and above) in all stages for high-REM nights. These differences do not seem to be salient for user 2 who does not  
662 show a significant trend of increasing REM % over time and only has one night just slightly above the REM percentage  
663 threshold of 30.

664 As we observe in Fig. 5B, the trends of model parameters across these recordings for user 2 show no significant trends  
665 in the corticocortical and thalamocortical circuit gains ( $x$  and  $y$ , respectively). But together with the increase in the  
666 REM percentage, the values of the thalamothalamic circuit gain ( $z$ ) are increased. This increase suggests that higher  
667 thalamo-thalamic inhibition is associated with the boosted REM sleep throughout those nights.

668 To further examine if these average-level trends are mediated by the imbalance in the sleep stages, in Fig. 5D., we  
669 caculated the average parameter values per sleep stage per night and plotted them against the REM percentage for that  
670 night. The inhibitory circuit gains associated with the thalamic relay nucleus ( $G_{srs}$  and  $G_{ese}$ ) see a trend of increased  
671 inhibition (more negative values) in all sleep stages in the nights with higher REM percentage. This corresponds to  
672 an increase in the thalamo-thalamic circuit gain  $z$  in these nights. These correlations are most pronounced in N1 and  
673 REM sleep stages. We also see moderate correlations of increased excitation and inhibition across all other cortical and  
674 thalamic gain parameters ( $G_{ee}$ ,  $G_{ei}$ ,  $G_{ese}$ ), but those values cancel each other out in the overall circuit gains  $x$  and  $y$ ,  
675 so they do not show a significant trend with REM percentage.

676 The distributions in Fig. 5C provide an overall view of these parameter distributions among the good vs. bad REM %  
677 nights. We see that nights with abnormal REM percentage have a different distributions in the  $xyz$  space, especially

678 seen in the  $xz$  and  $yz$  orthographic projections, with extensions in the  $z$  direction towards larger values in unhealthy  
679 REM % nights.

680 ***Nights of sleep with high REM percentage have stronger high-frequency power***

681 Another observable difference between the high-REM vs. low-REM nights is a clear increase in high-frequency power  
682 in the power spectra, as seen in Fig. 5A. As we argued earlier in this section, the combination of sleep quality parameters  
683 for this user points to a potential REM sleep disorder. In REM sleep behavior disorder (RBD) for instance, patients  
684 lose muscle atonia during REM sleep, which leads to them acting out their REM sleep mentations. Existence of  
685 an EMG rhythm in REM is the definitive diagnostic criteria for RBD [102, 103]. In this user, we have an increase  
686 in high-frequency power in high-REM nights, most prominently in REM sleep, which could be a result of muscle  
687 activity and EMG artifacts during sleep. In fact, in the mathematical model we use, there is an EMG term fitted to  
688 high-frequency power to mitigate the effects of EMG artifacts on the power spectra. The amplitude of this EMG term  
689 (the  $A_{EMG}$  parameter) is increased in the nights with higher REM percentage, as seen in Fig. 5B, further corroborating  
690 the suggested increase in muscle activity in high-REM nights.

691 **3.3.2 Model parameters are associated with markers of mental health**

692 In this step, the fitted parameters of the Wisconsin Sleep Cohort (WSC) were analyzed in conjunction with the  
693 biomarkers included in this dataset. Using Pearson's  $r$  test, the correlations between each of the 227 biomarkers and  
694 the average value per night for each of the 9 fitted model parameters were examined. To correct for the repeated  
695 pairwise correlation analysis, we used the False Discovery Rate (FDR) method introduced by Benjamini and Hochberg  
696 to correct the  $p$ -values in a ranked manner, taking into account the probable false positives in repeated testing [95, 104],  
697 bringing the  $p$ -value threshold for rejecting the null hypothesis from 0.05 to approximately 0.0396. There were 46  
698 significant correlations between the parameters, but they were all weak—with the highest  $|r|$ -value for any correlation  
699 being 0.16. The significant correlations between these health labels and average model parameters per night can be  
700 found in 2. Despite the weak correlations, discernible patterns arise when observing which specific parameters correlate  
701 with which biomarkers. For example, the connection strengths in the inhibitory thalamothalamic feedback loop ( $G_{srs}$ )  
702 and the the full thalamothalamic circuit ( $z$ ) exhibit correlations with the administration of various medication groups  
703 and neurochemicals, such as alpha blockers, selective serotonin reuptake inhibitors (SSRIs), diabetes medication, and  
704 alcohol. This could be attributed to the various efferent cholinergic [105, 106] and serotonergic [107] synapses that  
705 TRN receives, along with the complex calcium-dependent dynamics underlying its firing state and frequency [29],  
706 which would potentially be altered with the administration of these medications. The average thalamocortical circuit ( $y$ )  
707 exhibits significant correlations with biomarkers related to sleep quality and sleep debt, such as waking through sleep  
708 or daytime sleepiness. This is corroborated by evidence linking sleep deprivation to increased hyperexcitability and  
709 reduced specificity and functional connectivity in the thalamocortical connections [108, 109].

---

Table 2: Significant correlations between biomarkers and average parameters per night in WSC

Parameters	WSC Health Biomarker	<i>r</i> -value	<i>p</i> -value
$\beta$	Zung Depression Scale Item 13	-0.094	0.027
$\beta$	Wake up frequently during the night	0.111	0.009
$\beta$	Apnea-Hypopnea Index (REM)	0.101	0.017
$A_{EMG}$	Zung Depression Scale Item 20	-0.094	0.027
$A_{EMG}$	Percentage of stage 1 and 2 sleep among total sleep duration	0.092	0.030
$A_{EMG}$	Percentage of stage 3 and 4 sleep among total sleep duration	-0.111	0.009
$t_0$	State-Trait Anxiety Inventory (State Anxiety Subscale) Score	0.121	0.004
$t_0$	Self-reported weekday sleep duration in main sleep	-0.092	0.029
$t_0$	Self-reported daily sleep duration in main sleep	-0.090	0.034
$t_0$	Hypertension Medication, any	-0.100	0.018
$t_0$	Diuretic Medication	-0.112	0.008
$t_0$	Thyroid Medication	-0.090	0.033
$t_0$	Percentage of stage 1 sleep among total sleep duration	-0.114	0.007
$t_0$	Average Level of Oxygen Desaturation of Apnea and Hypopnea Event	-0.096	0.023
$G_{ei}$	Height	-0.089	0.036
$G_{ese}$	Caffeine intake, number of cups of coffee or tea per day	-0.092	0.030
$G_{ese}$	Wake up frequently during the night	0.090	0.034
$G_{esre}$	Zung Depression Scale Item 6	0.116	0.006
$G_{esre}$	Asthma Medication, control	-0.091	0.031
$G_{esre}$	Percentage of stage 1 and 2 sleep among total sleep duration	-0.101	0.017
$G_{srs}$	Zung Depression Scale Item 10	-0.128	0.003
$G_{srs}$	Alcohol consumption, number of beverages per week	0.126	0.003
$G_{srs}$	Frequency of gasping, choking or making snorting sound during sleep	-0.103	0.015
$G_{srs}$	Sleep Apnea	-0.133	0.002
$G_{srs}$	Asthma Medication, rescue	-0.105	0.013
$G_{srs}$	Antidepressant, SSRI	-0.093	0.028
$G_{srs}$	Alpha Blocker	-0.096	0.023
$G_{srs}$	Diabetes Medication/Insulin	-0.169	0.000
$G_{srs}$	Apnea-Hypopnea Index (REM)	0.098	0.020
$x$	Snoring frequency	-0.116	0.006
$y$	Zung Depression Scale Item 15	0.112	0.008
$y$	Wake up frequently during the night	0.122	0.004
$y$	Wake up too early	0.115	0.006
$y$	Excessive daytime sleepiness	0.111	0.009
$y$	Total days per month having any insomnia symptoms	0.095	0.025
$z$	Zung Depression Scale Item 10	0.115	0.007
$z$	Alcohol consumption, number of beverages per week	-0.107	0.012
$z$	Frequency of gasping, choking or making snorting sound during sleep	0.091	0.031
$z$	Sleep Apnea	0.125	0.003
$z$	Asthma Medication, any	0.094	0.027
$z$	Asthma Medication, rescue	0.136	0.001
$z$	Antidepressant, SSRI	0.101	0.017
$z$	Alpha Blocker	0.110	0.009
$z$	Diabetes Medication/Insulin	0.160	0.000
$z$	Apnea-Hypopnea Index (REM)	-0.098	0.020

710 **Selective Serotonin Reuptake Inhibitors (SSRIs) alter thalamocortical connectivity during deep NREM sleep**

711 Given the importance of changes in sleep as a comorbidity of many mental health disorders, we next focused on  
712 studying the correlations of the average physiological circuit parameters fitted over one night with the WSC variables  
713 related to mental health—namely trait and state anxiety, scores from the Zung self-rating depression scale [110], and  
714 antidepressant medication. The Zung index is a normalized integer score value between 25 to 100, wherein the scores  
715 between 50 and 59 are scored as mild depression, between 60 and 69 as moderate depression, and any value higher than  
716 70 as severe depression. Across our physiological model parameters we observed a weak but significant correlation  
717 ( $r = 0.10, p = 0.01$ ) between the consumption of SSRI antidepressant medication and the gain of the thalamothalamic  
718 circuit ( $z$ ).

719 We first tested whether the SSRI medication successfully reduces the severity of depression. In total, in 437 (78.60%) of  
720 the fitted recordings, the subject reported being on SSRI medication, and in the other 119 (21.40%), they were off SSRI  
721 medications. An independent-samples two-sided  $t$ -test demonstrates that the on-medication group has a significantly  
722 lower Zung index ( $t = -9.850, p < 0.001$ ) than the off-medication group.

723 Next, we compared the composition of the parameters in different stages of sleep between the on- and off-medication  
724 group. We repeated the analysis in Fig. 3 on the on-SSRIs and off-SSRIs groups separately as well, to see if the  
725 transition from W to N3 yields the same reduction in  $|y|$  and increase in  $x$  in both subgroups. Independent  $t$ -tests were  
726 used to compare the means of  $x$  and  $|y|$  between the two stages W and N3. In the off-medication group, we see a  
727 significant *depth of sleep* effect—where the reduction in  $|y|$  is significant and negative ( $t = -7.778, p < 0.001$ ) as is the  
728 increase in  $x$  ( $t = 2.004, p < 0.001$ ). In the on-medication group, both of these effects are significantly reduced, with  
729 no significant reduction in N3 thalamocortical circuit gains ( $t = -7.778, p = 0.997$ ) and very slight increase in the  $x$   
730 values ( $t = 2.045, p = 0.020$ ).

731 **Interactions between depression or SSRI biomarkers with parameters  $x, y, z$  are nonlinear**

732 We then attempted to see if the model parameters can be used to classify health labels directly, to test their potential  
733 standalone diagnostic use. We tried to predict whether the subject is on- or off-SSRI medication using the average or  
734 variance features of the WSC data, via classical machine learning approaches. We separated the data into training and  
735 test groups, with 80% of the fitted recordings in the training group and the other 20% in the testing group, with the  
736 on-SSRI group subsampled to match the size of the off-SSRI group. We then trained a linear kernel Support Vector  
737 Machine (SVM) to test if  $xyz$  in the on and off-medication groups are consistently separated using this support vector.  
738 The algorithm performed poorly at predicting the SSRI medication outcome. The linear-kernel SVM was not able to  
739 separate the two groups beyond chance level. This suggests that whole-night average parameter values are poor linear  
740 predictors of SSRI medication usage by themselves. For automated detection of the patterns observed in this paper  
741 using machine learning, we must utilize algorithms that can capture nonlinear relationships between the parameters and  
742 the health labels and the trajectories of change in the model parameters across a night of sleep, such as convolutional

743 neural networks (CNNs), or apply dimensionality-reduction techniques such as singular value decomposition (SVD) or  
744 Principal Component Analysis (PCA).

## 745 4 Discussion

746 In this work we aimed to study how brain activity changes across different sleep stages, in health vs. disease, and as  
747 a function of recording technology (research-grade vs. mobile EEG). EEG power spectral density was calculated in  
748 30s windows matching those of the hypnogram, delineating the frequency-domain characteristics of oscillatory and  
749 aperiodic background brain activity. Then, we used a neurophysiological modelling method introduced by Robinson  
750 et al. [45, 51, 89] to estimate various physiological parameters of corticothalamic brain circuits, and observe how  
751 these parameters change over sleep stages. Multiple sleep EEG datasets were employed to replicate our principal  
752 findings and to demonstrate the usage of this approach in various research and non-research scenarios, including most  
753 importantly, using at-home sleep EEG recordings from the consumer-grade sleep EEG headset Muse S. Changes in  
754 the  $1/f$ -parameterization of the power spectra was shown to be significantly correlated with the corticothalamic gain  
755 parameters linked to bottom-up thalamocortical drive of the cortical activity, with the exponents becoming larger with  
756 depth of sleep (Fig. 4 and Figs. S5 to S9). Deeper NREM sleep stages were also observed to undergo a severance  
757 of effective bottom-up thalamocortical control, signified by reduced thalamocortical circuit gains ( $|y|$ ) and increased  
758 cortical excitability, signified by elevated corticocortical circuit gain values ( $x$ ) (Fig. 3 and Fig. S4). Administration of  
759 SSRI medication was observed to block this disintegration of corticothalamic connections in deep sleep. We additionally  
760 studied a case of an individual conducting repeated at-home sleep EEG recordings via Muse S, presenting with a  
761 REM parasomnia, associated with increased high-frequency EEG activity in the power spectrum, and an increase in  
762 thalamo-thalamic inhibition in the model parameter space. In summary, it was demonstrated that this physiological  
763 modelling approach can effectively integrate the periodic & aperiodic components of the EEG power spectra more  
764 robustly than common PSD analysis techniques and provide a reliable and physiologically explainable parameterization  
765 of those spectra in health & disease, and for the brain's response to a treatment.

### 766 4.1 Key Results

#### 767 *Thalamic relay excitation increases the $1/f$ slope*

768 A central result that was consistent across most of the analyzed datasets was that whereas connectivity strengths for  
769 cortico-cortical connections ( $G_{ee}$  and  $G_{ei}$ ,  $x$ ) had negligible associations with the fitted  $1/f$  offsets and exponents,  
770 strong correlations with  $1/f$  features were seen for connections involving thalamic units ( $G_{ese}$ ,  $G_{esre}$ , and  $G_{srs}$ ). The  
771 pattern is such that the higher the value of the gains (either excitatory or inhibitory), the bigger the exponent of the  $1/f$   
772 component, and so the more steep the background trend.

773 Previous literature points to the importance of the thalamic reticular nucleus as a regulator of excitatory thalamic nuclei  
774 activity, including relay nuclei [111, 29, 28]. This thalamic control loop attenuates the excitatory drive from thalamic

775 relay nuclei to the cortex, thereby regulating the activity of the cortical neural populations underlying measured EEG  
776 signals.

777 As described in the 2 section, in the Robinson model, the thalamic relay nuclei ( $s$ ) constitutes the main excitatory output  
778 of the thalamus, whose influence is balanced by the thalamic reticular nucleus ( $r$ ) that implements a negative feedback  
779 loop, extinguishing the thalamic relay excitatory output. The loop gain  $G_{srs}$  gain parameter summarizes how the  
780 balance between these two units ( $s \rightarrow r \rightarrow s$ ) enables this inhibitory feedback. One implication of our modelling results  
781 is that increased thalamo-thalamic inhibitory activity, signified by increases in inhibitory thalamic gains, flattens the  $1/f$   
782 spectrum by inhibiting the thalamocortical circuit driving the cortex. When this inhibition is removed, the network-level  
783 disinhibition in the cortex leads to a more steep  $1/f$  slope. Previous authors (Gao et al. [20], Lombardi et al. [99] have  
784 suggested that higher  $1/f$  exponents can be regarded as a criterion for higher cortical inhibition, driven not by thalamic  
785 but by cortical inhibitory populations, whereas our findings concentrate on the bottom-up thalamo-cortical axis of  
786 communication and how increases in its absolute gains lead to increased  $1/f$  exponents.

787 A caveat for this model, as noted by Abeysuriya and Robinson [89], is that the gain ( $G$ ) parameters are dependent on both  
788 the steady-state neural field and the synaptic strength of each population (per Eqn.(15)) and changes in either parameter  
789 can lead to a rise in the gain parameters, yielding infinite solutions for the exact delineation of these two parameters.  
790 Furthermore, another simplification in this model is the assumption of random outgoing synaptic connectivity, leading  
791 to  $G_{ei} = G_{ii}$  and  $G_{ie} = G_{ii}$ , which may imbalance this cortical E/I balance estimation.

792 ***Thalamo-cortical disinhibition during the progression from wake to deep sleep***

793 Using the neurophysiological model of thalamocortical system, we demonstrated that with the transition from wake to  
794 sleep, concurrent with an increase in the  $1/f$  exponents, the values of the corticothalamic circuit ( $x$ ) increase and the  
795 absolute values of the thalamo-cortical circuit gain ( $y$ ) approach 0 (Fig. 3C). As we move from lighter sleep to deeper  
796 NREM sleep (from wakefulness to sleep stage N1, and then to N2, and then N3), the values of  $x$  increase further, such  
797 that in N3, their values are distributed very narrowly, close to the maximum value of 1.0. Concurrently, the value of  $|y|$   
798 decreases, such that in N3, it has a narrow distribution close to 0 (both in Figure 4C). As noted, the values of  $y$  depend  
799 not only on the existence of thalamocortical activity, but also on the nature of its contribution (i.e. whether it influences  
800 inhibitory or excitatory activity from the thalamus to the cortex) [51]. In this sense, the deeper stages of NREM sleep,  
801 especially N3, involve increased cortical excitability, but at the same time, the thalamocortical population is insensitive  
802 to activity propagated through the thalamus. This highlights prior work by Nir et al. [40] demonstrating that EEG slow  
803 wave activity during deep NREM sleep is regionally and not globally synchronized, and that the oscillatory phases vary  
804 spatially over the cortical surface. Additionally, Massimini et al. [41] demonstrate that these slow waves can be locally  
805 interrupted and entrained using transcranial magnetic stimulation (TMS) at 1 Hz, suggesting a cortically-generated  
806 dynamic where local stimulation has the capacity to disrupt them. This pattern of dis-facilitation and dis-inhibition in  
807 N3 are in line with previous work using biophysical models denoting a reduction in thalamic excitation or inhibition in  
808 the brain in slow wave sleep [32] despite an increase in cortical synaptic strength [38, 112, 113]. Other work using

809 neural mass models of thalamocortical circuitry by Müller et al. [114] has recently demonstrated the importance of  
810 the thalamus in maintaining the E/I balance in the cortex. They posit that adding a diffuse "one-to-all" connection  
811 term between the thalamus and the cortex, which is supported by empirical observations of the thalamic matrix nuclei  
812 helps recruit and dissolve the ensembles needed for cortical processing, and increases the transfer entropy from the  
813 thalamus to the cortex. They show that the effects of these matrix nuclei are highest in wakefulness and are decreased  
814 when modelling the effects of propofol anesthesia. This separation between conscious and unconscious states is in line  
815 with our observations regarding the bottom-up thalamocortical excitation or inhibition. Namely, we show that deeper  
816 sleep is correlated with the lack of large scale entrainment of the cortical activity by the thalamus, and the work by  
817 Müller et al. [114] delineates the other side of this same phenomenon that awake EEG corresponds to increases in the  
818 thalamocortical diffuse connectivity, driving the cortical activity from the bottom up. Further work utilizing the added  
819 thalamic nuclei in their work on the trajectories of activity in sleep can delineate the potential effects of matrix thalamus  
820 on sleep physiology as well.

821 ***The sign of  $y$  depends on the dataset, rather than the immediate power spectra***

822 We found the mean and the mode of the fitted values for the circuit gains ( $x$ ,  $y$ , and  $z$ ) to be slightly different in various  
823 datasets. This could be justified by the different amount of time spent in different sleep stages (Fig. 2A) and thus the  
824 different oscillatory regimes dominating the data (Fig. 2C).

825 Despite the observation in Abeysuriya et al. [51] reporting excitatory thalamocortical regimes noted by positive  $y$  values  
826 in wakefulness decreases to negative values with the transition from wake to sleep, we observed that the numerical  
827 sign of  $y$  depends more on the datasets used than the stages of sleep. We noted the frequent "sign" of  $y$  to changes  
828 across datasets, irrelevant of wakefulness vs. sleep. For instance, 72.38% of all  $y$  values among 120,855 wake epochs  
829 in the EDF-X dataset were negative and 66.20% of all 2,119 epochs during sleep in the Nap-EEG dataset were positive.  
830 Hence, our work suggests a more nuanced take where the transition from wake to sleep shifts to a more inhibitory  
831 regime, marked by reductions in  $y$  along the depth of sleep axis, but that does not reflect an overall domination of  
832 bottom up inhibition as soon as sleep is initiated. Future work comparing the topography of these effects can shine light  
833 on the network-level variations in such changes.

834 ***Repeated at-home recordings using mobile EEG can help us better observe parasomnias and modelling can help us  
835 understand the physiological basis of these conditions***

836 We showed in this study an example of how repeated at-home recordings using mobile EEG can help us characterize  
837 the changes in EEG for a subject with a REM parasomnia. The repeated recordings allowed us to observe that the REM  
838 parasomnia is indeed consistent across nights and not a one-off sporadic event for the subject. For this subject, the  
839 EEG from the nights of high REM percentage (above 30%) had a flatter power spectrum, and the model parameters  
840 suggested a change in thalamothalamic gains in those nights.

---

841 The model seemed to fit more negative values for the gain parameters  $G_{esre}$  and  $G_{srs}$  in those nights. As observed in  
842 Fig. 4B, increasing these two gain parameters generate spectra with flatter  $1/f$  components and higher alpha, beta,  
843 and high-frequency components. In other words, our model represents an increase in thalamo-thalamic inhibition with  
844 such a shape of the power spectra, and in the case of the parasomnias subject, has fitted power spectra with flatter  $1/f$   
845 components in the high-REM nights with higher thalamo-thalamic inhibition.

846 In this case, the increased high-frequency EEG activity in the REM parasomnia nights could be caused by a possible  
847 increase in the EMG-related artifacts in the EEG, as a result of increased muscle activity and loss of REM atonia,  
848 which is a characteristic of REM behaviour disorder. In this case, we also do not see all of the classic power spectral  
849 features of RBD, such as general slowing of the EEG, or general and widespread disruptions of N3 sleep. This is all  
850 further complicated by the great heterogeneity in the presentations of RBD for younger vs. older adults, and in the  
851 context of alpha-synucleinopathies [103, 115]. We highlight that these observations from one user are not complete,  
852 and nothing could be definitely diagnosed without observing the subject's EMG during REM sleep, which is the  
853 definitive diagnostic criterion. But this observed trend is promising for organizing focused future studies on REM  
854 parasomnias using mobile EEG from repeated recordings. In future work, the other actigraphy data that is already  
855 collected from many of the common consumer-grade sleep EEG headsets like Muse S can be combined with these  
856 power spectra to help with the diagnosis of REM parasomnias.

## 857 4.2 Limitations and Next steps

858 In this work we have focused primarily on changes in model parameters associated with transitions between sleep stages.  
859 However, these stages are far from the only physiologically-significant features we can extract from sleep EEG datasets.  
860 Other phenomena of interest could for instance be the dynamics of alpha activity in the final minutes of transitioning  
861 from wakefulness to sleep, which prior work has found to be associated with pathologies such as insomnia and sleep  
862 deprivation [116–118].

## 863 *Studying sleep spindles*

864 Another area of interest for future work that the framework presented here can be well suited to studying is transient  
865 oscillatory events in EEG traces such as sleep spindles and k-complexes. Abeysuriya et al. [49] utilize this model of the  
866 EEG power spectra to generate the power spectral density resulting from spindle generation. In this work the authors  
867 use stability analysis of the corticothalamic system to predict the nonlinear harmonic frequencies of the spindle peaks.  
868 In a follow-up study [50], they then demonstrated the existence of these spindle harmonics in empirical EEG data, as  
869 well robust fitting of an extended version of the model. In this case, the nonlinear harmonic frequencies of the spindle  
870 are resulting from the thalamo-thalamic feedback loop, and differ from the linear harmonic frequencies associated  
871 with the primary alpha and beta peaks. This study of the predicted harmonics in EEG power spectra can be useful for  
872 comparing the specific underlying corticothalamic connections generating such activity.

---

873 A long line of work on murine sleep EEG has demonstrated the importance of the corticothalamic system in generating  
874 sleep spindles. Empirically, shifts in the excitatory and inhibitory firing rates of various neural populations have been  
875 implicated in the generation of sleep spindles, initiated by a transition in the thalamic reticular nucleus [28, 119]. The  
876 circuit mechanisms and underlying mathematical structure of spindle generation in these detailed thalamic models  
877 [120] and the coarser-grained corticothalamic models [50, 49] may be related, but are not identical. They could be best  
878 understood as either complementary or competing candidate theories of this prominent phenomenon observed in human  
879 sleep EEG. An important direction for future work should be to compare and characterize the relevant parallels between  
880 these two frameworks, such as relating the models' excitation and inhibition parameters to the  $1/f$  EEG features across  
881 sleep stages described in this study.

882 The current work does not include any in-depth assessment of sleep spindles, as only one of the datasets used here  
883 (Nap-EEG) contained consistent spindle events with expert labelling in the EEG data. Separation of the spindles in  
884 the other datasets requires expert or machine learning-based detection of the spindles, which was out of the scope  
885 of the present work. Furthermore, sleep spindles start and end in short spans of approximately 2 seconds, which is  
886 much shorter than our standard power spectrum epochs of 30 seconds. The window sizes would therefore need to  
887 be substantially shortened to accommodate spindle-oriented analyses, which would in turn deleteriously increase the  
888 proportion of noise-driven peaks in the spectra, making model fitting less stable and consistent. In future work, we will  
889 study spindles as they appear in mobile EEG data specifically, and characterize changes in their occurrence, frequency,  
890 length, amplitude, etc over sleep stages. These data can then be used to inform fitting of the corticothalamic model to the  
891 spindle PSDs, per [50, 49], thereby mapping these empirically-observed changes to transitions in the model parameters.

892 As we have indicated, sleep spindles are oscillatory events which begin, rise, decay, and then conclude in a well-  
893 characterized and parameterizable fashion. It is also notable that the phase and frequency of the spindles can vary  
894 spatially. In this study, due to computational limitations and variation in the data sets, we were restricted to fitting the  
895 power spectra to only one EEG channel. A logical next step would be to individually fit *all* EEG channels from the  
896 datasets, and analyze the parameters in the channel space, or to implement the spatial modes in the analytic power  
897 spectrum ( $k$ ). The topography and spatial modes of these trajectories are topics of active interest in the field [121], and  
898 observing their changes in wakefulness and sleep in health and disease, especially in the context of mobile EEG, has  
899 clear scientific and clinical value.

900 In the future we will also consider transform-based machine learning, in which the transform is not merely a pre-  
901 processor but is also itself part of a neural network [122, 123], as well as phase-based methods [124]. Indeed, much of  
902 the important information in oscillatory activity during sleep is arguably better represented in terms of phase space, as  
903 well as scale space, phase scale, and the chirplet transform [122, 123], because sleep stages are often characterized  
904 by changes in frequency (acceleration of phase) [125–127]. Chirplet-based analytical approaches potentially offer a  
905 more biologically sympathetic perspective on neural signal analysis, which can aid corticothalamic modelling of sleep  
906 neurophysiology by better capturing time-varying frequency modulations in the EEG [128].

907 **Implementation of this pipeline in large cohorts**

908 Combining the above-outlined strategy with *de-novo* at-home sleep recordings using the Muse S headset, with a larger  
909 sample size than studied here, is a promising extension of the present work. In particular, this has major potential  
910 for studying sleep EEG features and the physiological underpinnings at-scale - both in terms of number of subjects  
911 (hundreds to thousands) and number of sleep sessions per subject (dozens or more). Adding biomarkers related to sleep  
912 quality and general health, for example through surveys or integration with other wearable biometric devices, would  
913 also be of great utility in delineating the physiological basis of those biomarkers.

914 In the present work, simple features of the distribution of 9 fitted corticothalamic model parameters across a night  
915 of sleep (such as mean, mode, and standard deviation) were used. In future work, using data-driven dimensionality  
916 reduction techniques to identify underlying sub-structures within these parameter values may prove an effective use of  
917 the physiological model outputs to help predict the health status and outcomes, both in extant datasets such as WSC  
918 [78], as well as new Muse S recordings with surveys described above.

919 **4.3 Conclusions**

920 In summary, our work has showcased the adaptability and reliability of this neurophysiological model [51, 89] for  
921 generating the trajectory of brain states during a sleep recording, utilizing a range of EEG data with various setups  
922 and recorded in various locales. This method adds another degree of physiological interpretability to the observations  
923 made based on EEG time series and power spectra. A robust interplay was observed between the aperiodic and periodic  
924 power spectral components, fitted model parameters, and their stage-dependent dynamics. This method can be effective  
925 for comparing sleep EEG between and among subjects and inferring latent health or disease states.

926 **5 Disclosure Statement**

927 MAJ and CAA are full-time employees of InteraXon Inc. at the time of writing.

928 **6 Acknowledgements**

929 **Computing:** The computing infrastructure for this work included the CAMH Specialized Computing Cluster (SCC)  
930 and the cluster Narval at Calcul Québec, part of the Digital Research Alliance of Canada. The SCC is funded by the  
931 Canada Foundation for Innovation's (CFI) Research Hospital Fund. These platforms allowed for quick and robust  
932 large-scale model fitting to entire datasets and whole-dataset analyses.

933 **Grants:** This work was completed as a part of T.M.'s MSc thesis at the Institute of Medical Science (IMS), Temerty  
934 Faculty of Medicine, University of Toronto. Project funding and stipend for this degree were provided via UoT  
935 EMHSeed. The project was further supported by the CAMH Discovery Fund and the Krembil Foundation. The  
936 Wisconsin Sleep Cohort (WSC) Study and data was supported by the U.S. National Institutes of Health, National

937 Heart, Lung, and Blood Institute (R01HL62252), National Institute on Aging (R01AG036838, R01AG058680), and  
938 the National Center for Research Resources (1UL1RR025011). The National Sleep Research Resource (NSRR)  
939 was supported by the U.S. National Institutes of Health, National Heart Lung and Blood Institute (R24 HL114473,  
940 75N92019R002).

941 **Author contributions** (*in alphabetic order*): **CA**: Methodology, Resources, Data Curation, **DM**: Writing - Original  
942 Draft, Visualization, **JDG**: Conceptualization, Methodology, Software, Resources, Data Curation, Writing - Original  
943 Draft, Writing - Review & Editing, Visualization, Supervision, Project administration, Funding acquisition, **KK**:  
944 Writing - Review & Editing, **MAJ**: Methodology, Data Curation, **MPO**: Visualization, Writing - Review & Editing,  
945 **SB**: Writing - Review & Editing, **SH**: Writing - Original Draft, **SLH**: Supervision, Project administration, Funding  
946 acquisition, Writing - Review & Editing, **SM**: Funding acquisition, Writing - Review & Editing, **TM**: Conceptualization,  
947 Methodology, Software, Validation, Formal analysis, Investigation, Resources, Data Curation, Writing - Original Draft,  
948 Writing - Review & Editing, Visualization, **ZW**: Writing - Original Draft.

## 949 Data and Resource Availability

- 950 1. The Sleep EDF-Extended (EDF-X) dataset version 1.0.0 used in this work is available on PhysioNet at  
951 <https://physionet.org/content/sleep-edfx/>, and described in Kemp et al. [70].
- 952 2. Dreem-Open-Datasets (DOD-H & DOD-O) and their annotations are available openly online. Full in-  
953 structions on acquiring the data are included at <https://github.com/Dreem-Organization/dreem-learning-open>.
- 954 3. The Wisconsin Sleep Cohort (WSC) dataset is available on the National Sleep Research Resource (NSRR)  
955 [77] at <https://sleepdata.org/datasets/wsc> and can be accessed openly for academic research.
- 956 4. The Nap-EEG dataset is available via the Open Science Foundation (OSF) at <https://osf.io/chav7/>.  
957 Further information about the data is included by the authors at [https://github.com/nmningmei/Get\\_Sleep\\_data](https://github.com/nmningmei/Get_Sleep_data).
- 958 5. The MCMC model fitting algorithm implemented on MATLAB is available at <https://github.com/BrainDynamicsUSYD/braintrak>.
- 959 6. The analysis and visualization code used in this paper is included in this GitHub Repository: [https://github.com/GriffithsLab/MorshedzadehEtAl2024\\_sleep-eeg-nft](https://github.com/GriffithsLab/MorshedzadehEtAl2024_sleep-eeg-nft).

## 964 References

- 965 [1] Chiara Cirelli and Giulio Tononi. Is sleep essential? *PLoS Biol*, 6(8):e216, 2008. doi: 10.1371/journal.pbio.0060216.
- 966 [2] Serge Daan, DG Beersma, and Alexander A Borbély. Timing of human sleep: recovery process gated by a  
967 circadian pacemaker. *Am J Physiol Regul Integr Comp Physiol*, 246(2):R161–R183, 1984. doi: 10.1152/ajpregu.  
968 1984.246.2.r161.
- 969 [3] Lulu Xie, Hongyi Kang, Qiwu Xu, Michael J. Chen, Yonghong Liao, Meenakshisundaram Thiagarajan, John  
970 O'Donnell, Daniel J. Christensen, Charles Nicholson, Jeffrey J. Iliff, Takahiro Takano, Rashid Deane, and  
971 Maiken Nedergaard. Sleep Drives Metabolite Clearance from the Adult Brain. *Science*, 342(6156):373–377,  
972 October 2013. ISSN 0036-8075. doi: 10.1126/science.1241224.
- 973 [4] Emmanuel Mignot. Why we sleep: the temporal organization of recovery. *PloS Biol*, 6(4):e106, 2008. doi:  
974 10.1371/journal.pbio.0060106.
- 975 [5] Wilfredo Blanco, Catia M. Pereira, Vinicius R. Cota, Annie C. Souza, César Rennó-Costa, Sharlene Santos,  
976 Gabriella Dias, Ana M. G. Guerreiro, Adriano B. L. Tort, Adrião D. Neto, and Sidarta Ribeiro. Synaptic  
977 Homeostasis and Restructuring across the Sleep-Wake Cycle. *PLoS Comput Biol*, 11(5):e1004241, May 2015.  
978 ISSN 1553-7358. doi: 10.1371/journal.pcbi.1004241.

980 [6] Le Shi, Si-Jing Chen, Meng-Ying Ma, Yan-Ping Bao, Ying Han, Yu-Mei Wang, Jie Shi, Michael V. Vitiello, and  
981 Lin Lu. Sleep disturbances increase the risk of dementia: A systematic review and meta-analysis. *Sleep Med*  
982 *Rev*, 40:4–16, August 2018. ISSN 1087-0792. doi: 10.1016/j.smrv.2017.06.010.

983 [7] Yo-El S Ju, Aleksandar Videnovic, and Bradley V Vaughn. Comorbid sleep disturbances in neurologic disorders.  
984 *Continuum (Minneapolis Minn)*, 23(4):1117–1131, 2017. doi: 10.1212/con.0000000000000501.

985 [8] Daniela Minecan, Alamelu Natarajan, Mary Marzec, and Beth Malow. Relationship of epileptic seizures to sleep  
986 stage and sleep depth. *Sleep*, 25(8):899–904, December 2002. ISSN 0161-8105. doi: 10.1093/sleep/25.8.56.  
987 URL <https://pubmed.ncbi.nlm.nih.gov/12489898>.

988 [9] David Nutt, Sue Wilson, and Louise Paterson. Sleep disorders as core symptoms of depression. *Dialogues Clin*  
989 *Neurosci*, 10(3):329, September 2008. doi: 10.31887/DCNS.2008.10.3/dnutt.

990 [10] G. Stores. Clinical diagnosis and misdiagnosis of sleep disorders. *J Neurol Neurosurg Psychiatry*, 78(12):1293,  
991 December 2007. doi: 10.1136/jnnp.2006.111179.

992 [11] J Zeitlhofer, P Anderer, S Obergottsberger, P Schimicek, S Lurger, E Marschnigg, B Saletu, and L Deecke.  
993 Topographic mapping of EEG during sleep. *Brain Topogr*, 6:123–129, 1993. doi: 10.1007/bf01191077.

994 [12] Conrad Iber and American Academy of Sleep Medicine. *The AASM manual for the scoring of sleep and*  
995 *associated events: rules, terminology and technical specifications*. American Academy of Sleep Medicine,  
996 Westchester, IL, 2007. OCLC: 438914652.

997 [13] Anthony Kales, Allan Rechtschaffen, Los Angeles University of California, and National Institute of Neurological  
998 Diseases and Blindness (U.S.). *A manual of standardized terminology, techniques and scoring system for sleep*  
999 *stages of human subjects*. NIH publication. United States Government Printing Office, Washington, DC, 1968.  
1000 doi: 10.1016/0013-4694(69)90021-2.

1001 [14] Charles Bae and Nancy Foldvary-Schaefer. The use of sleep studies in neurological practice. *Semin Neurol*, 24  
1002 (3):237–248, September 2004. ISSN 0271-8235. doi: 10.1055/s-2004-835072.

1003 [15] Axel Steiger and Mayumi Kimura. Wake and sleep EEG provide biomarkers in depression. *J Psychiatr Res*, 44  
1004 (4):242–252, March 2010. ISSN 1879-1379. doi: 10.1016/j.jpsychires.2009.08.013.

1005 [16] Adam Wichniak, Aleksandra Wierzbicka, and Wojciech Jernajczyk. Sleep as a biomarker for depression.  
1006 *Int Rev Psychiatry*, October 2013. URL <https://www.tandfonline.com/doi/full/10.3109/09540261.2013.812067>.

1008 [17] José Haba-Rubio, Pedro Marques-Vidal, Daniela Andries, Nadia Tobback, Martin Preisig, Peter Vollenweider,  
1009 Gérard Waeber, Gianina Luca, Mehdi Tafti, and Raphaël Heinzer. Objective sleep structure and cardiovascular  
1010 risk factors in the general population: the HypnoLaus Study. *Sleep*, 38(3):391–400, March 2015. ISSN  
1011 1550-9109. doi: 10.5665/sleep.4496.

1012 [18] Daphne Chylinski, Christian Berthomier, Eric Lambot, Sonia Frenette, Marie Brandewinder, Julie Carrier, Gilles  
1013 Vandewalle, and Vincenzo Muto. Variability of sleep stage scoring in late midlife and early old age. *J Sleep Res*,  
1014 31(1):e13424, 2022.

1015 [19] Magdy Younes, Jill Raneri, and Patrick Hanly. Staging sleep in polysomnograms: analysis of inter-scorer  
1016 variability. *J Clin Sleep Med*, 12(6):885–894, 2016. doi: 10.5664/jcsm.5894.

1017 [20] Richard Gao, Erik J Peterson, and Bradley Voytek. Inferring synaptic excitation/inhibition balance from field  
1018 potentials. *NeuroImage*, 158:70–78, 2017. doi: 10.1016/j.neuroimage.2017.06.078.

1019 [21] Kusum Thuwal, Arpan Banerjee, and Dipanjan Roy. Aperiodic and Periodic Components of Ongoing Oscil-  
1020 latory Brain Dynamics Link Distinct Functional Aspects of Cognition across Adult Lifespan. *eNeuro*, 8(5):  
1021 ENEURO.0224–21.2021, September 2021. doi: 10.1523/eneuro.0224-21.2021.

1022 [22] Guang Ouyang, Andrea Hildebrandt, Florian Schmitz, and Christoph S. Herrmann. Decomposing alpha and 1/f  
1023 brain activities reveals their differential associations with cognitive processing speed. *NeuroImage*, 205:116304,  
1024 January 2020. doi: 10.1016/j.neuroimage.2019.116304.

1025 [23] Gert Pfurtscheller and Christa Neuper. *Movement and ERD/ERS*, pages 191–206. Springer US, 2003. doi:  
1026 10.1007/978-1-4615-0189-3\_12.

1027 [24] Thomas E Scammell, Elda Arrigoni, and Jonathan O Lipton. Neural circuitry of wakefulness and sleep. *Neuron*,  
1028 93(4):747–765, 2017. doi: 10.1016/j.neuron.2017.01.014.

1029 [25] Eric R. Kandel, James H. Schwartz, Thomas M. Jessell, Steven A. Siegelbaum, and A. J. Hudspeth. *Principles  
1030 of Neural Science, Fifth Edition*. McGraw Hill Professional, October 2012. ISBN 978-0-07-181001-2. Google-  
1031 Books-ID: Z2yVUTnIQuC.

1032 [26] Jae Myeong Kang, Seo-Eun Cho, Jong Youn Moon, Soo In Kim, Jong Won Kim, and Seung-Gul Kang. Difference  
1033 in spectral power density of sleep electroencephalography between individuals without insomnia and frequent  
1034 hypnotic users with insomnia complaints. *Sci Rep*, 12(1):2117, 2022. doi: 10.1038/s41598-022-05378-6.

1035 [27] Yuval Nir, Marcello Massimini, Melanie Boly, and Giulio Tononi. Sleep and Consciousness. In Andrea Eugenio  
1036 Cavanna, Andrea Nani, Hal Blumenfeld, and Steven Laureys, editors, *Neuroimaging of Consciousness*, pages  
1037 133–182. Springer, Berlin, Heidelberg, 2013. ISBN 978-3-642-37580-4. doi: 10.1007/978-3-642-37580-4\_9.  
1038 URL <https://doi.org/10.1007/978-3-642-37580-4%5F9>.

1039 [28] Mircea Steriade, David A. McCormick, and Terrence J. Sejnowski. Thalamocortical Oscillations in the Sleeping  
1040 and Aroused Brain. *Science*, 262(5134):679–685, oct 29 1993. doi: 10.1126/science.8235588. URL <http://dx.doi.org/10.1126/SCIENCE.8235588>.

1041 [29] David A. McCormick and Thierry Bal. SLEEP AND AROUSAL: Thalamocortical Mechanisms. *Annu Rev  
1042 Neurosci*, 20(1):185–215, March 1997. doi: 10.1146/annurev.neuro.20.1.185. URL <http://dx.doi.org/10.1146/ANNUREV.NEURO.20.1.185>.

1045 [30] PA Robinson, CJ Rennie, JJ Wright, H Bahramali, E Gordon, and DL Rowe. Prediction of electroencephalo-  
1046 graphic spectra from neurophysiology. *Phys Rev E*, 63(2):021903, 2001. doi: 10.1103/physreve.63.021903.

1047 [31] Igor Timofeev, François Grenier, and Mircea Steriade. Disfacilitation and active inhibition in the neocortex  
1048 during the natural sleep-wake cycle: An intracellular study. *Proc. Natl. Acad. Sci. U.S.A.*, 98(4):1924–1929,  
1049 February 2001. doi: 10.1073/pnas.98.4.1924.

1050 [32] Sean Hill and Giulio Tononi. Modeling sleep and wakefulness in the thalamocortical system. *J Neurophysiol*, 93  
1051 (3):1671–1698, 2005. doi: 10.1152/jn.00915.2004.

1052 [33] Giulio Tononi and Chiara Cirelli. Sleep function and synaptic homeostasis. *Sleep Med Rev*, 10(1):49–62, 2006.  
1053 doi: 10.1016/j.smrv.2005.05.002.

1054 [34] Antoine R. Adamantidis, Carolina Gutierrez Herrera, and Thomas C. Gent. Oscillating circuitries in the sleeping  
1055 brain. *Nat Rev Neurosci*, 20(12):746–762, December 2019. ISSN 1471-0048. doi: 10.1038/s41583-019-0223-4.

1056 [35] Tadao Hori. Spatiotemporal Changes of EEG Activity During Waking-Sleeping Transition Period. *Int J Neurosci*,  
1057 January 1985. ISSN 1129-3354. doi: 10.3109/00207458509149139. URL <https://www.tandfonline.com/doi/abs/10.3109/00207458509149139>.

1058 [36] Bence Schneider, Orsolya Szalárdy, Péter P. Ujma, Péter Simor, Ferenc Gombos, Ilona Kovács, Martin Dresler,  
1059 and Róbert Bódizs. Scale-free and oscillatory spectral measures of sleep stages in humans. *Front Neuroinf*, 16:  
1060 989262, October 2022. ISSN 1662-5196. doi: 10.3389/fninf.2022.989262.

1061 [37] Leslie D Claar, Irene Rembado, Jacqulyn R Kuyat, Simone Russo, Lydia C Marks, Shawn R Olsen, and Christof  
1062 Koch. Cortico-thalamo-cortical interactions modulate electrically evoked EEG responses in mice. *eLife*, 12:  
1063 RP84630, jun 2023. ISSN 2050-084X. doi: 10.7554/eLife.84630. URL <https://doi.org/10.7554/eLife.84630>.

1064 [38] Steve K. Esser, Sean Hill, and Giulio Tononi. Breakdown of Effective Connectivity During Slow Wave  
1065 Sleep: Investigating the Mechanism Underlying a Cortical Gate Using Large-Scale Modeling. *J Neurophysiol*,  
1066 October 2009. doi: 10.1152/jn.00059.2009. URL <https://journals.physiology.org/doi/full/10.1152/jn.00059.2009>.

1067 [39] Thien Thanh Dang-Vu, Manuel Schabus, Martin Desseilles, Geneviève Albouy, Mélanie Boly, Annabelle  
1068 Darsaud, Steffen Gais, Géraldine Rauchs, Virginie Sterpenich, Gilles Vandewalle, Julie Carrier, Gustave Moonen,  
1069 Evelyne Balteau, Christian Degueldre, André Luxen, Christophe Phillips, and Pierre Maquet. Spontaneous  
1070 neural activity during human slow wave sleep. *Proc Natl Acad Sci*, 105(39):15160–15165, September 2008.  
1071 ISSN 0027-8424, 1091-6490. doi: 10.1073/pnas.0801819105. URL <https://pnas.org/doi/full/10.1073/pnas.0801819105>.

1072 [40] Yuval Nir, Richard J. Staba, Thomas Andrillon, Vladyslav V. Vyazovskiy, Chiara Cirelli, Itzhak Fried, and  
1073 Giulio Tononi. Regional Slow Waves and Spindles in Human Sleep. *Neuron*, 70(1):153–169, April 2011. ISSN  
1074 0896-6273. doi: 10.1016/j.neuron.2011.02.043.

1075

1079 [41] Marcello Massimini, Fabio Ferrarelli, Steve K. Esser, Brady A. Riedner, Reto Huber, Michael Murphy, Michael J.  
1080 Peterson, and Giulio Tononi. Triggering sleep slow waves by transcranial magnetic stimulation. *Proc Natl  
1081 Acad Sci*, 104(20):8496–8501, May 2007. ISSN 0027-8424, 1091-6490. doi: 10.1073/pnas.0702495104. URL  
1082 <https://doi.org/10.1073/pnas.0702495104>.

1083 [42] Yina Wei, Giri P. Krishnan, Lisa Marshall, Thomas Martinetz, and Maxim Bazhenov. Stimulation Augments  
1084 Spike Sequence Replay and Memory Consolidation during Slow-Wave Sleep. *J Neurosci*, 40(4):811–824,  
1085 January 2020. ISSN 0270-6474. doi: 10.1523/JNEUROSCI.1427-19.2019.

1086 [43] PA Robinson, CJ Rennie, and DL Rowe. Dynamics of large-scale brain activity in normal arousal states and  
1087 epileptic seizures. *Phys Rev E*, 65(4):041924, 2002. doi: 10.1103/physreve.65.041924.

1088 [44] Christopher J Rennie, Peter A Robinson, and James J Wright. Unified neurophysical model of EEG spectra and  
1089 evoked potentials. *Biol Cybern*, 86(6):457–471, 2002. doi: 10.1007/s00422-002-0310-9.

1090 [45] PA Robinson, CJ Rennie, DL Rowe, SC O’Connor, JJ Wright, E Gordon, and RW Whitehouse. Neurophysical  
1091 modeling of brain dynamics. *Neuropsychopharmacology*, 28(1):S74–S79, 2003. doi: 10.1038/sj.npp.1300143.

1092 [46] Tara Babaie-Janvier and Peter A Robinson. Neural field theory of evoked response potentials with attentional  
1093 gain dynamics. *Front Hum Neurosci*, 14:293, 2020. doi: 10.3389/fnhum.2020.00293.

1094 [47] Peter A Robinson, Natasha C Gabay, and Tara Babaie-Janvier. Neural Field Theory of Evoked Response  
1095 Sequences and Mismatch Negativity With Adaptation. *Front Hum Neurosci*, 15:655505, 2021. doi: 10.3389/  
1096 fnhum.2021.655505.

1097 [48] PA Robinson, RW Whitehouse, and CJ Rennie. Nonuniform corticothalamic continuum model of elec-  
1098 troencephalographic spectra with application to split-alpha peaks. *Phys Rev E*, 68(2):021922, 2003. doi:  
1099 10.1103/physreve.68.021922.

1100 [49] Romesh G Abeysuriya, Chris J Rennie, and Peter A Robinson. Prediction and verification of nonlinear sleep  
1101 spindle harmonic oscillations. *J Theor Biol*, 344:70–77, 2014. doi: 10.1016/j.jtbi.2013.11.013.

1102 [50] RG Abeysuriya, CJ Rennie, PA Robinson, and JW Kim. Experimental observation of a theoretically predicted  
1103 nonlinear sleep spindle harmonic in human EEG. *Clin Neurophysiol*, 125(10):2016–2023, 2014. doi: 10.1016/j.  
1104 clinph.2014.01.025.

1105 [51] Romesh G. Abeysuriya, Christopher J. Rennie, and Peter A. Robinson. Physiologically based arousal state  
1106 estimation and dynamics. *J Neurosci Methods*, 253, 06 2015. doi: 10.1016/j.jneumeth.2015.06.002.

1107 [52] Maurice Abou Jaoude, Aravind Ravi, Jiansheng Niu, Hubert Banville, Nicolas Florez Torres, and Christopher  
1108 Aimone. Automated Sleep Staging on Wearable EEG Enables Sleep Analysis at Scale. In *2023 11th International  
1109 IEEE/EMBS Conference on Neural Engineering (NER)*, pages 1–4. IEEE, 2023. doi: 10.1109/NER52421.2023.  
1110 10123829. URL <https://ieeexplore.ieee.org/abstract/document/10123829>.

1111 [53] Pierrick J Arnal, Valentin Thorey, Eden Debellemaniere, Michael E Ballard, Albert Bou Hernandez, Antoine  
1112 Guillot, Hugo Jourde, Mason Harris, Mathias Guillard, Pascal Van Beers, et al. The Dreem Headband compared

1113 to polysomnography for electroencephalographic signal acquisition and sleep staging. *Sleep*, 43(11):zsaa097,  
1114 2020. doi: 10.1093/sleep/zsaa097.

1115 [54] Magdy Younes, Marc Soferman, Wayne Thompson, and Eleni Giannouli. Performance of a new portable wireless  
1116 sleep monitor. *J Clin Sleep Med*, 13(2):245–258, February 2017. ISSN 1550-9397. doi: 10.5664/jcsm.6456.

1117 [55] Noralie Krepel, Tommy Egtberts, Emma Touré-Cuq, Pierre Bouny, and Martijn Arns. Evaluation of the  
1118 URGOnight Tele-neurofeedback Device: An Open-label Feasibility Study with Follow-up. *Appl Psychophysiol  
1119 Biofeedback*, 47(1):43–51, March 2022. ISSN 1573-3270. doi: 10.1007/s10484-021-09525-z.

1120 [56] M. Wälti, M. Thielen, M. Melnykowycz, E. Gasparri, and E. Meier. Preliminary validation of in-ear EEG against  
1121 PSG system for sleep staging. *Sleep Med*, 100:S22, December 2022. ISSN 1389-9457. doi: 10.1016/j.sleep.  
1122 2022.05.073.

1123 [57] Scott Bressler, Ryan Neely, Ryan M Yost, and David Wang. A randomized controlled trial of alpha phase-locked  
1124 auditory stimulation to treat symptoms of sleep onset insomnia. *Sci Rep*, 14(1):13039, June 2024. ISSN  
1125 2045-2322. doi: 10.1038/s41598-024-63385-1.

1126 [58] Johan Newell, Olivier Mairesse, Paul Verbanck, and Daniel Neu. Is a one-night stay in the lab really enough  
1127 to conclude? First-night effect and night-to-night variability in polysomnographic recordings among different  
1128 clinical population samples. *Psychiatry Res*, 200(2-3):795–801, December 2012. ISSN 1872-7123. doi:  
1129 10.1016/j.psychres.2012.07.045.

1130 [59] Hylton E. Molzof, Sarah E. Emert, Joshua Tutek, Mazheruddin M. Mulla, Kenneth L. Lichstein, Daniel J. Taylor,  
1131 and Brant W. Riedel. Intraindividual sleep variability and its association with insomnia identity and poor sleep.  
1132 *Sleep Med*, 52:58–66, December 2018. ISSN 1389-9457. doi: 10.1016/j.sleep.2018.08.014.

1133 [60] Sarah M. Inkellis, Sonia Ancoli-Israel, Jennifer D. Thomas, and Rakesh Bhattacharjee. Elevated risk of depression  
1134 among adolescents presenting with sleep disorders. *J Clin Sleep Med*, 17(4):675–683, April 2021. ISSN 1550-  
1135 9389, 1550-9397. doi: 10.5664/jcsm.8996.

1136 [61] Norifumi Tsuno, Alain Berset, and Karen Ritchie. Sleep and Depression. *J Clin Psychiatry*, 66(10):19685,  
1137 October 2005. ISSN 0160-6689.

1138 [62] Mi-Mi Zhang, Yan Ma, Lan-Ting Du, Ke Wang, Zhe Li, Weili Zhu, Yu-Hui Sun, Lin Lu, Yan-Ping Bao, and  
1139 Su-Xia Li. Sleep disorders and non-sleep circadian disorders predict depression: A systematic review and  
1140 meta-analysis of longitudinal studies. *Neurosci Biobehav Rev*, 134:104532, March 2022. ISSN 0149-7634. doi:  
1141 10.1016/j.neubiorev.2022.104532.

1142 [63] Antonio Zadra and D. C. Donderi. Nightmares and bad dreams: Their prevalence and relationship to well-being.  
1143 *J Abnorm Psychol*, 109(2):273–281, 2000. ISSN 1939-1846. doi: 10.1037/0021-843X.109.2.273.

1144 [64] Nicholas Pesant and Antonio Zadra. Dream content and psychological well-being: A longitudinal study of  
1145 the continuity hypothesis. *J Clin Psychol*, 62(1):111–121, January 2006. ISSN 0021-9762, 1097-4679. doi:  
1146 10.1002/jclp.20212.

1147 [65] William Wong, Thomas Andrillon, Nicolas Decat, Valdas Noreika, Katja Valli, Jennifer Windt, and Naotsugu  
1148 Tsuchiya. The DREAM database, February 2023. URL <https://bridges.monash.edu/articles/dataset/The%5FDREAM%5Fdatabase/22133105/2>.

1149

1150 [66] Stefan Lang, Davide Momi, Artur Vetkas, Brendan Santyr, Andrew Z. Yang, Suneil K. Kalia, John D. Griffiths,  
1151 and Andres Lozano. Computational modeling of whole-brain dynamics: A review of neurosurgical applications.  
1152 *J Neurosurg*, 140(1):218–230, June 2023. ISSN 1933-0693, 0022-3085. doi: 10.3171/2023.5.JNS23250.

1153 [67] V. K. Jirsa, T. Proix, D. Perdikis, M. M. Woodman, H. Wang, J. Gonzalez-Martinez, C. Bernard, C. Bénar,  
1154 M. Guye, P. Chauvel, and F. Bartolomei. The Virtual Epileptic Patient: Individualized whole-brain models of  
1155 epilepsy spread. *NeuroImage*, 145:377–388, January 2017. ISSN 1053-8119. doi: 10.1016/j.neuroimage.2016.  
1156 04.049.

1157 [68] Viktor Jirsa, Huifang Wang, Paul Triebkorn, Meysam Hashemi, Jayant Jha, Jorge Gonzalez-Martinez, Maxime  
1158 Guye, Julia Makhlova, and Fabrice Bartolomei. Personalised virtual brain models in epilepsy. *Lancet Neurol*,  
1159 22(5):443–454, May 2023. ISSN 1474-4465. doi: 10.1016/S1474-4422(23)00008-X.

1160 [69] Magali Haas, Diane Stephenson, Klaus Romero, Mark Forrest Gordon, Neta Zach, Hugo Geerts, and Brain  
1161 Health Modeling Initiative (BHMI). Big data to smart data in Alzheimer’s disease: Real-world examples  
1162 of advanced modeling and simulation. *Alzheimers Dement*, 12(9):1022–1030, 2016. ISSN 1552-5279. doi:  
1163 10.1016/j.jalz.2016.05.005.

1164 [70] Bob Kemp, Aeilko H Zwinderman, Bert Tuk, Hilbert AC Kamphuisen, and Josefien JL Oberrye. Analysis of a  
1165 sleep-dependent neuronal feedback loop: the slow-wave microcontinuity of the EEG. *IEEE Trans Biomed Eng*,  
1166 47(9):1185–1194, 2000. doi: 10.1109/10.867928.

1167 [71] Bob Kemp, A Zwinderman, B Tuk, H Kamphuisen, and J Oberryé. Sleep-EDF Database Expanded, 2018. URL  
1168 <https://www.physionet.org/content/sleep-edfx/1.0.0/>.

1169 [72] Ary L Goldberger, Luis AN Amaral, Leon Glass, Jeffrey M Hausdorff, Plamen Ch Ivanov, Roger G Mark,  
1170 Joseph E Mietus, George B Moody, Chung-Kang Peng, and H Eugene Stanley. PhysioBank, PhysioToolkit,  
1171 and PhysioNet: components of a new research resource for complex physiologic signals. *Circulation*, 101(23):  
1172 e215–e220, 2000. doi: 10.1161/01.cir.101.23.e215.

1173 [73] Antoine Guillot, Fabien Sauvet, Emmanuel H During, and Valentin Thorey. Dreem open datasets: Multi-scored  
1174 sleep datasets to compare human and automated sleep staging. *IEEE Trans Neural Syst Rehabilitation Eng*, 28  
1175 (9):1955–1965, 2020. doi: 10.1109/tnsre.2020.3011181.

1176 [74] Valentin Thorey, Simon Kerns, and Antoine Guillot. Dreem-Organization/dreem-learning-open, February  
1177 2021. URL <https://github.com/Dreem-Organization/dreem-learning-open>. original-  
1178 date: 2019-11-05T16:44:38Z.

1179 [75] Ning Mei, Michael D Grossberg, Kenneth Ng, Karen T Navarro, and Timothy M Ellmore. A high-density scalp  
1180 EEG dataset acquired during brief naps after a visual working memory task. *Data Brief*, 18:1513–1519, 2018.  
1181 doi: 10.1016/j.dib.2018.04.073.

1182 [76] Timothy Ellmore, Ning Mei, Kenneth Ng, and Karen Tatiana Navarro. Nap EEG, July 2016. URL <https://osf.io/chav7/>. Publisher: OSF.

1184 [77] Guo-Qiang Zhang, Licong Cui, Remo Mueller, Shiqiang Tao, Matthew Kim, Michael Rueschman, Sara Mariani,  
1185 Daniel Mobley, and Susan Redline. The National Sleep Research Resource: towards a sleep data commons. *J  
1186 Am Med Inform Assoc*, 25(10):1351–1358, 2018. doi: 10.1145/3233547.3233725.

1187 [78] Terry Young, Mari Palta, Jerome Dempsey, Paul E Peppard, F Javier Nieto, and K Mae Hla. Burden of sleep  
1188 apnea: rationale, design, and major findings of the Wisconsin Sleep Cohort study. *WMJ*, 108(5):246, 2009.

1189 [79] Christoph Guger, Gunther Krausz, Brendan Z. Allison, and Guenter Edlinger. Comparison of Dry and Gel Based  
1190 Electrodes for P300 Brain–Computer Interfaces. *Front Neurosci*, 6:25155, May 2012. ISSN 1662-453X. doi:  
1191 10.3389/fnins.2012.00060.

1192 [80] Alexandre Gramfort, Martin Luessi, Eric Larson, Denis A Engemann, Daniel Strohmeier, Christian Brodbeck,  
1193 Roman Goj, Mainak Jas, Teon Brooks, Lauri Parkkonen, et al. MEG and EEG data analysis with MNE-Python.  
1194 *Front Neurosci*, 7:267, 2013. doi: 10.3389/fnins.2013.00267.

1195 [81] Peter Welch. The use of fast Fourier transform for the estimation of power spectra: a method based on time  
1196 averaging over short, modified periodograms. *IEEE Trans Audio Electroacoust*, 15(2):70–73, 1967. doi:  
1197 10.1109/tau.1967.1161901.

1198 [82] Jie Cui and Willy Wong. Optimal window length in the windowed adaptive chirplet analysis of visual evoked  
1199 potentials. In *2006 International Conference of the IEEE Engineering in Medicine and Biology Society*, pages  
1200 4580–4583. IEEE, 2006.

1201 [83] Thomas Donoghue, Matar Haller, Erik J Peterson, Paroma Varma, Priyadarshini Sebastian, Richard Gao, Torben  
1202 Noto, Antonio H Lara, Joni D Wallis, Robert T Knight, et al. Parameterizing neural power spectra into periodic  
1203 and aperiodic components. *Nat Neuro*, 23(12):1655–1665, 2020. doi: 10.1038/s41593-020-00744-x.

1204 [84] Raphael Vallat and Matthew P. Walker. An open-source, high-performance tool for automated sleep staging.  
1205 *eLife*, October 2021. doi: 10.7554/eLife.70092.

1206 [85] Ramesh Srinivasan, Don M Tucker, and Michael Murias. Estimating the spatial Nyquist of the human EEG. *Beh  
1207 Res Meth Instr Comp*, 30(1):8–19, 1998. doi: 10.3758/bf03209412.

1208 [86] Suresh Muthukumaraswamy. High-frequency brain activity and muscle artifacts in MEG/EEG: A review and  
1209 recommendations. *Front Hum Neurosci*, 7:47068, April 2013. ISSN 1662-5161. doi: 10.3389/fnhum.2013.00138.

1210 [87] Federico Barban, Michela Chiappalone, Gaia Bonassi, Dante Mantini, and Marianna Semprini. Yet another  
1211 artefact rejection study: an exploration of cleaning methods for biological and neuromodulatory noise. *J Neural  
1212 Eng*, 18(4):0460c2, August 2021. ISSN 1741-2552. doi: 10.1088/1741-2552/ac01fe.

1213 [88] Donald L Rowe, Peter A Robinson, and Christopher J Rennie. Estimation of neurophysiological parameters from  
1214 the waking EEG using a biophysical model of brain dynamics. *Journal of theoretical biology*, 231(3):413–433,  
1215 2004. doi: 10.1016/j.jtbi.2004.07.004.

1216 [89] RG Abeysuriya and PA Robinson. Real-time automated EEG tracking of brain states using neural field theory. *J  
1217 Neurosci Methods*, 258:28–45, 2016. doi: 10.1016/j.jneumeth.2015.09.026.

1218 [90] Romesh Abeysuriya. BrainDynamicsUSYD/braintrak, January 2019. URL <https://github.com/BrainDynamicsUSYD/braintrak>. original-date: 2015-04-01T22:37:43Z.

1220 [91] Ushtar Amin, Fábio A. Nascimento, Ioannis Karakis, Donald Schomer, and Selim R. Benbadis. Normal variants  
1221 and artifacts: Importance in EEG interpretation. *Epileptic Disord*, 25(5):591–648, jul 2023.

1222 [92] Jose Antonio Uríguen and Begoña García-Zapirain. EEG artifact removal—state-of-the-art and guidelines. *J  
1223 Neural Eng*, 12(3):031001, April 2015. ISSN 1741-2552. doi: 10.1088/1741-2560/12/3/031001.

1224 [93] Scott I Vrieze. Model selection and psychological theory: a discussion of the differences between the Akaike  
1225 information criterion (AIC) and the Bayesian information criterion (BIC). *Psychol Methods*, 17(2):228, 2012.  
1226 doi: 10.1037/a0027127.

1227 [94] Pauli Virtanen, Ralf Gommers, Travis E. Oliphant, Matt Haberland, Tyler Reddy, David Cournapeau, Evgeni  
1228 Burovski, Pearu Peterson, Warren Weckesser, Jonathan Bright, Stéfan J. van der Walt, Matthew Brett, Joshua  
1229 Wilson, K. Jarrod Millman, Nikolay Mayorov, Andrew R. J. Nelson, Eric Jones, Robert Kern, Eric Larson, C J  
1230 Carey, İlhan Polat, Yu Feng, Eric W. Moore, Jake VanderPlas, Denis Laxalde, Josef Perktold, Robert Cimrman,  
1231 Ian Henriksen, E. A. Quintero, Charles R. Harris, Anne M. Archibald, Antônio H. Ribeiro, Fabian Pedregosa,  
1232 Paul van Mulbregt, and SciPy 1.0 Contributors. SciPy 1.0: Fundamental Algorithms for Scientific Computing in  
1233 Python. *Nat Meth*, 17:261–272, 2020. doi: 10.1038/s41592-019-0686-2.

1234 [95] Yoav Benjamini and Yosef Hochberg. Controlling the False Discovery Rate: A Practical and Powerful Approach  
1235 to Multiple Testing. *J R Stat Soc Series B Stat Methodol*, 57(1):289–300, 1995. ISSN 00359246. doi:  
1236 10.1111/j.2517-6161.1995.tb02031.x. URL <http://www.jstor.org/stable/2346101>.

1237 [96] F. Pedregosa, G. Varoquaux, A. Gramfort, V. Michel, B. Thirion, O. Grisel, M. Blondel, P. Prettenhofer, R. Weiss,  
1238 V. Dubourg, J. Vanderplas, A. Passos, D. Cournapeau, M. Brucher, M. Perrot, and E. Duchesnay. Scikit-learn:  
1239 Machine Learning in Python. *J Mach Learn Res*, 12:2825–2830, 2011.

1240 [97] Mary A. Carskadon and William C. Dement. Normal Human Sleep: An Overview. In *Principles and Practice of  
1241 Sleep Medicine (Sixth Edition)*, pages 15–24.e3. Elsevier, Waltham, MA, USA, January 2017. ISBN 978-0-323-  
1242 24288-2. doi: 10.1016/B978-0-323-24288-2.00002-7.

1243 [98] Sophie Desjardins, Sylvie Lapierre, Carol Hudon, and Alain Desgagné. Factors involved in sleep efficiency: a  
1244 population-based study of community-dwelling elderly persons. *Sleep*, 42(5):zsz038, 2019. doi: 10.1093/sleep/  
1245 zsz038.

1246 [99] Fabrizio Lombardi, Hans J Herrmann, and Lucilla de Arcangelis. Balance of excitation and inhibition determines  
1247 1/f power spectrum in neuronal networks. *Chaos*, 27(4):047402, 2017. doi: 10.1063/1.4979043.

1248 [100] Winston Haynes. *Bonferroni Correction*, pages 154–154. Springer New York, New York, NY, 2013.  
1249 ISBN 978-1-4419-9863-7. doi: 10.1007/978-1-4419-9863-7\_1213. URL [https://doi.org/10.1007/978-1-4419-9863-7\\_1213](https://doi.org/10.1007/978-1-4419-9863-7_1213).

1250 [101] Mark I. Boulos, Trevor Jairam, Tetyana Kendzerska, James Im, Anastasia Mekhail, and Brian J. Murray. Normal  
1251 polysomnography parameters in healthy adults: A systematic review and meta-analysis. *Lancet Respir Med*, 7  
1252 (6):533–543, June 2019. ISSN 2213-2600, 2213-2619. doi: 10.1016/S2213-2600(19)30057-8.

1253 [102] Yuichi Inoue, Taeko Sasai, and Koichi Hirata. Electroencephalographic Finding in Idiopathic REM Sleep  
1254 Behavior Disorder. *Neuropsychobiology*, 71(1):25–33, 2015. ISSN 0302-282X, 1423-0224. doi: 10.1159/000363343.

1255 [103] Melanie Bergmann, Birgit Högl, and Ambra Stefani. Clinical neurophysiology of REM parasomnias: Diagnostic  
1256 aspects and insights into pathophysiology. *Clin Neurophysiol Pract*, 9:53, January 2024. doi: 10.1016/j.cnp.2023.10.003.

1257 [104] Winston Haynes. *Bonferroni Correction*, pages 154–154. Springer New York, New York, NY, 2013.  
1258 ISBN 978-1-4419-9863-7. doi: 10.1007/978-1-4419-9863-7\_1213. URL [https://doi.org/10.1007/978-1-4419-9863-7\\_1213](https://doi.org/10.1007/978-1-4419-9863-7_1213).

1259 [105] Qiang Li, Jiang-Ling Song, Si-Hui Li, M. Brandon Westover, and Rui Zhang. Effects of Cholinergic Neuromodulation on Thalamocortical Rhythms During NREM Sleep: A Model Study. *Front Comp Neurosci*, 13, 2020.  
1260 ISSN 1662-5188.

1261 [106] David A. McCormick. Chapter 36: Actions of acetylcholine in the cerebral cortex and thalamus and implications  
1262 for function. In *Progress in Brain Research*, volume 98, pages 303–308. Elsevier, Waltham, MA, USA, January  
1263 1993. doi: 10.1016/S0079-6123(08)62412-7.

1264 [107] José J. Rodríguez, Harun N. Noristani, Walter B. Hoover, Stephanie B. Linley, and Robert P. Vertes. Serotonergic  
1265 projections and serotonin receptor expression in the reticular nucleus of the thalamus in the rat. *Synapse*, 65(9):  
1266 919–928, September 2011. ISSN 1098-2396. doi: 10.1002/syn.20920.

1267 [108] Margaret N. Shouse. Sleep deprivation increases thalamocortical excitability in the somatomotor pathway,  
1268 especially during seizure-prone sleep or awakening states in feline seizure models. *Exp. Neurol.*, 99(3):664–677,  
1269 March 1988. ISSN 0014-4886. doi: 10.1016/0014-4886(88)90183-5.

1270 [109] Yongcong Shao, Lubin Wang, Enmao Ye, Xiao Jin, Wei Ni, Yue Yang, Bo Wen, Dewen Hu, and Zheng Yang.  
1271 Decreased Thalamocortical Functional Connectivity after 36 Hours of Total Sleep Deprivation: Evidence from  
1272 Resting State fMRI. *PLoS One*, 8(10), 2013. doi: 10.1371/journal.pone.0078830.

1273 [110] William WK Zung. A self-rating depression scale. *Arch Gen Psychiatry*, 12(1):63–70, 1965. doi: 10.1037/t04095-000.

1274

1275

1276

1277

1278

1279

1280 [111] RW Guillery, SL Feig, and DA Lozsadi. Paying attention to the thalamic reticular nucleus. *Trends Neurosci*, 21  
1281 (1):28–32, 1998. doi: 10.1016/s0166-2236(97)01157-0.

1282 [112] Brady A. Riedner, Vladislav V. Vyazovskiy, Reto Huber, Marcello Massimini, Steve Esser, Michael Murphy, and  
1283 Giulio Tononi. Sleep Homeostasis and Cortical Synchronization: III. A High-Density EEG Study of Sleep Slow  
1284 Waves in Humans. *Sleep*, 30(12):1643–1657, December 2007. ISSN 0161-8105. doi: 10.1093/sleep/30.12.1643.

1285 [113] Vladislav V. Vyazovskiy, Brady A. Riedner, Chiara Cirelli, and Giulio Tononi. Sleep Homeostasis and Cortical  
1286 Synchronization: II. A Local Field Potential Study of Sleep Slow Waves in the Rat. *Sleep*, 30(12):1631–1642,  
1287 December 2007. ISSN 0161-8105. doi: 10.1093/sleep/30.12.1631.

1288 [114] Eli J. Müller, Brandon R. Munn, Michelle J. Redinbaugh, Joseph Lizier, Michael Breakspear, Yuri B. Saalmann,  
1289 and James M. Shine. The non-specific matrix thalamus facilitates the cortical information processing modes  
1290 relevant for conscious awareness. *Cell Rep*, 42(8), August 2023. ISSN 2211-1247. doi: 10.1016/j.celrep.2023.  
1291 112844.

1292 [115] Adeel A. Memon, Corina Catiul, Zachary Irwin, Jennifer Pilkington, Raima A. Memon, Allen Joop, Kimberly H.  
1293 Wood, Gary Cutter, Svjetlana Miocinovic, and Amy W. Amara. Quantitative sleep electroencephalogram and  
1294 cognitive performance in Parkinson’s disease with and without rapid eye movement sleep behavior disorder. *Frnt  
1295 Neurol*, 14, September 2023. ISSN 1664-2295. doi: 10.3389/fneur.2023.1223974.

1296 [116] Nazanin Biabani, Adam Birdseye, Sean Higgins, Alessio Delogu, Jan Rosenzweig, Zoran Cvetkovic, Alexander  
1297 Nesbitt, Panagis Drakatos, Joerg Steier, Veena Kumari, David O’Regan, and Ivana Rosenzweig. The neurophysi-  
1298 ologic landscape of the sleep onset: a systematic review. *J Thorac Dis*, 15(8), August 2023. ISSN 2077-6624.  
1299 doi: 10.21037/jtd-23-325.

1300 [117] Justus T. C. Schwabedal, Maik Riedl, Thomas Penzel, and Niels Wessel. Alpha-wave frequency characteristics  
1301 in health and insomnia during sleep. *J Sleep Res*, 25(3):278–286, June 2016. ISSN 1365-2869. doi: 10.1111/jsr.  
1302 12372.

1303 [118] Jintao Wu, Qianxiang Zhou, Jiaxuan Li, Yang Chen, Shuyu Shao, and Yi Xiao. Decreased resting-state alpha-  
1304 band activation and functional connectivity after sleep deprivation. *Sci Rep*, 11(1):1–10, January 2021. ISSN  
1305 2045-2322. doi: 10.1038/s41598-020-79816-8.

1306 [119] Pablo Fuentealba, Igor Timofeev, and Mircea Steriade. Prolonged hyperpolarizing potentials precede spindle  
1307 oscillations in the thalamic reticular nucleus. *Proc Natl Acad Sci*, 101(26):9816–9821, 2004. doi: 10.1073/pnas.  
1308 0402761101.

1309 [120] Elisabetta Iavarone, Jane Simko, Ying Shi, Marine Bertschy, María García-Amado, Polina Litvak, Anna-Kristin  
1310 Kaufmann, Christian O’Reilly, Oren Amsalem, Marwan Abdellah, et al. Thalamic control of sensory processing  
1311 and spindles in a biophysical somatosensory thalamorecipient circuit model of wakefulness and sleep. *Cell Rep*,  
1312 42(3), 2023. doi: 10.1016/j.celrep.2023.112200.

1313 [121] James C. Pang, Kevin M. Aquino, Marianne Oldehinkel, Peter A. Robinson, Ben D. Fulcher, Michael Breakspear,  
1314 and Alex Fornito. Geometric constraints on human brain function. *Nature*, 618(7965):566–574, June 2023.  
1315 ISSN 1476-4687. doi: 10.1038/s41586-023-06098-1.

1316 [122] Jie Cui and Willy Wong. Investigation of short-term changes in visual evoked potentials with windowed adaptive  
1317 chirplet transform. *IEEE Transactions on Biomedical Engineering*, 55(4):1449–1454, 2008.

1318 [123] Steve Mann and Simon Haykin. Adaptive chirplet: an adaptive generalized wavelet-like transform. In *Adaptive  
1319 Signal Processing*, volume 1565, pages 402–413. SPIE, 1991.

1320 [124] Gerald B Folland. *Harmonic analysis in phase space*. Number 122. Princeton university press, 1989.

1321 [125] Diego Z Carvalho, Günther JL Gerhardt, Guilherme Dellagustin, Emerson L de Santa-Helena, Ney Lemke,  
1322 Alan Z Segal, and Suzana V Schönwald. Loss of sleep spindle frequency deceleration in obstructive sleep apnea.  
1323 *Clinical Neurophysiology*, 125(2):306–312, 2014.

1324 [126] Diego Carvalho, Suzana Schönwald, Guilherme Dellagustin, Emerson de Santa-Helena, Ney Lemke, and Gunther  
1325 Gerhardt. Sleep spindle frequency modulation (chirp) in obstructive sleep apnea (p04. 025), 2012.

1326 [127] Suzana V Schönwald, Diego Z Carvalho, Guilherme Dellagustin, Emerson L de Santa-Helena, and Günther JL  
1327 Gerhardt. Quantifying chirp in sleep spindles. *Journal of Neuroscience Methods*, 197(1):158–164, 2011.

1328 [128] Rafael Toledo Fernandes de Souza, Günther Johannes Lewczuk Gerhardt, Suzana Veiga Schönwald, José Luiz  
1329 Rybarczyk-Filho, and Ney Lemke. Synchronization and propagation of global sleep spindles. *PLoS One*, 11(3):  
1330 e0151369, 2016.

1331 **List of Figures**

1332 1	Method for fitting the sleep EEG power spectra to the model. . . . .	9
1333 2	Comparison of sleep architecture metrics and power spectral features across datasets . . . . .	17
1334 3	Tracking the changes in the parameters in different sleep stages in the Nap-EEG dataset . . . . .	20
1335 4	Correlation between model parameters and the shape of the power spectra . . . . .	23
1336 5	Sleep quality metrics in repeated nights . . . . .	27